DES 09-131
SFB-CPP/10-032

DESY 09–131
SFB-CPP/10–032
May 2010

QCD Analysis of Polarized Deep Inelastic Scattering Data

Johannes Blümlein and Helmut Böttcher

Deutsches Elektronen Synchrotron, DESY

Platanenallee 6, D–15738 Zeuthen, Germany

Abstract

A QCD analysis of the world data on polarized deep inelastic scattering is presented in next–to–leading order, including the heavy flavor Wilson coefficient in leading order in the fixed flavor number scheme. New parameterizations are derived for the quark and gluon distributions and the value of $\alpha_s(M_z^2)$ is determined. The impact of the variation of both the renormalization and factorization scales on the distributions and the value of α_s is studied. We obtain $\alpha_s^{\rm NLO}(M_Z^2) = 0.1132 \begin{array}{c}+0.0056\\-0.0095\end{array}$. The first moments of the polarized twist–2 parton distribution functions are calculated with correlated errors to allow for comparisons with results from lattice QCD simulations. Potential higher twist contributions to the structure function $g_1(x, Q^2)$ are determined and found to be compatible with zero both for proton and deuteron targets.

1 Introduction

The short–distance structure of the nucleon spin still consists a developing field. Nucleons as composite fermions obtain their spin in terms of a superposition of the spins and orbital angular momenta of their constituents, the quarks and gluons. It came as a surprise when the European Muon Collaboration (EMC) published its result [1] more than 20 years ago, which showed that the quarks do contribute only by a small fraction to the nucleon's spin. The obvious conclusion was to assume that the spin of the gluons and the orbital angular momenta of all constituents have to account for the missing fraction. This result initiated activities worldwide both on the experimental and the theoretical side in order to understand this spin puzzle and, finally, the spin structure of the nucleon.

Experiments performed at CERN, SLAC, DESY and JLAB [1–15] have contributed a vast amount of experimental data on inclusive polarized deeply inelastic lepton–nucleon scattering (DIS) during the last years. The main interest in measuring the short distance structure of polarized nucleons has somewhat moved from determining the first moments of the twist–2 parton distributions to the extraction of their x-dependence in the measured region and their scaling violations due to QCD–evolution. At large enough four-momentum transfer $Q^2 = -q^2$, the structure function $g_1(x, Q^2)$ mainly receives twist–2 contributions[1] and is related to the polarized twist–2 parton distributions.

In the present paper a QCD analysis of the polarized deep–inelastic world data is performed at next-to-leading order (NLO). Due to a larger set of new data which has become available recently the present analysis extends and updates earlier investigations [9, 15, 17–26]. In the QCD-fit we determine the flavor singlet and non-singlet contributions of the polarized parton densities together with the QCD-scale $\Lambda_{\rm QCD}$ with correlated errors. The measurement of the strong coupling constant $\alpha_s(M_Z^2)$ from polarized deep-inelastic data does not reach the same precision as in the unpolarized case [27–30] since the measurement is based on an asymmetry and the present analysis is performed in NLO. However, a consistent analysis requires the determination of the QCD-scale $\Lambda_{\rm QCD}$ along with the parameters of the non-perturbative input distributions. Also, it is interesting to see which value of $\alpha_s(M_Z^2)$ is obtained in comparison to other deep–inelastic analyzes. At a given scale Q^2 the Mellin moments of the parton distribution functions can be calculated under some assumptions on their extrapolation outside the measured region towards small and very large values of the Bjorken variable x. We also analyze, to which extend the present data contain higher twist contributions.

The paper is organized as follows. In Section 2 the basic formalism is lined out. The data analysis is described in Section 3. In Section 4 details of the fit are given and Section 5 deals with the error analysis. The results of the QCD analysis are presented in Section 6. In Section 7 we determine potential higher twist contributions and Section 8 contains the conclusions. In the Appendix we describe the `FORTRAN`-code through which the polarized parton distributions and structure functions can be obtained for numerical analyzes.

2 Basic Formalism

The twist–2 contributions to the spin–dependent structure function $g_1(x, Q^2)$ are given in terms of a Mellin convolution of the polarized singlet $\Delta\Sigma$, the gluon ΔG and the flavor non-singlet

[1] Twist–3 contributions are connected by target mass effects, cf. [16].

(NS) $\Delta q_i^{\rm NS}$ densities with the corresponding Wilson coefficient functions ΔC_i^A by

$$g_1(x,Q^2) = \frac{1}{2}\sum_{i=1}^{N_f} e_i^2 \int_x^1 \frac{dz}{z}\left[\frac{1}{N_f}\Delta\Sigma\left(\frac{x}{z},\mu_f^2\right)\Delta C_q^S\left(z,\frac{Q^2}{\mu_f^2}\right) + \Delta G\left(\frac{x}{z},\mu_f^2\right)\Delta C_G\left(z,\frac{Q^2}{\mu_f^2},\frac{m_c^2}{Q^2}\right) + \Delta q_i^{NS}\left(\frac{x}{z},\mu_f^2\right)\Delta C_q^{NS}\left(z,\frac{Q^2}{\mu_f^2}\right)\right] . \quad (1)$$

Here x is the Bjorken variable, e_i denotes the charge of the ith quark flavor in units of the elementary charge and N_f is the number of light flavors. The scale μ_f denotes the factorization scale which is introduced to remove the collinear singularities from the partonic structure functions. In addition to the factorization scale there is the renormalization scale μ_r of the strong coupling constant $\alpha_s(\mu_r^2)$. The gluonic Wilson coefficient ΔC_G accounts for the massless as well the massive contributions due to charm quark production for $W^2 > (2m_c + m_N)^2$ with $m_c = 1.5$ GeV, [31], at first order. [2] For the implementation of the Wilson coefficients in Mellin space we refer to [33]. The parton densities and the Wilson coefficient functions are dependent on these scales and obey corresponding renormalization group equations, while the structure function $g_1(x,Q^2)$, as a physical observable, is independent of the choice of both scales μ_f^2 and μ_r^2.

The polarized singlet and non–singlet parton densities which occur in Eq. (1) are expressed by the individual quark flavor contributions as

$$\Delta\Sigma\left(z,\mu_f^2\right) = \sum_{i=1}^{N_f}\left[\Delta q_i\left(z,\mu_f^2\right) + \Delta\bar{q}_i\left(z,\mu_f^2\right)\right] , \quad (2)$$

$$\Delta q_i^{NS}\left(z,\mu_f^2\right) = \Delta q_i\left(z,\mu_f^2\right) + \Delta\bar{q}_i\left(z,\mu_f^2\right) - \frac{1}{N_f}\Delta\Sigma\left(z,\mu_f^2\right) , \quad (3)$$

where Δq_i denotes the polarized quark distribution of the ith light flavor.

The running coupling constant α_s is obtained as the solution of

$$\frac{d\alpha_s(\mu_r^2)}{d\log(\mu_r^2)} = -\beta_0\alpha_s^2(\mu_r^2) - \beta_1\alpha_s^3(\mu_r^2) + O(\alpha_s^4) , \quad (4)$$

where, in the $\overline{\rm MS}$–scheme, the coefficients of the β–function are given by

$$\beta_0 = \frac{11}{3}C_A - \frac{4}{3}T_F N_f ,$$
$$\beta_1 = \frac{34}{3}C_A^2 - \frac{20}{3}C_A T_F N_f - 4C_F T_F N_f , \quad (5)$$

with the color factors $C_A = 3$, $T_F = 1/2$, and $C_F = 4/3$. Matching of the scale $\Lambda_{\rm QCD}^{N_f}$ is performed at $Q^2 = m_c^2,\ m_b^2$, with $m_c = 1.5$ GeV and $m_b = 4.5$ GeV.

In the present analysis the spin–dependent structure functions $g_1^p(x,Q^2)$ and $g_1^n(x,Q^2)$ will be considered referring to $N_f = 3$ light partonic flavors, i.e. $i = u,d,s$. The spin–dependent structure function $g_1^d(x,Q^2)$ is represented in terms of $g_1^p(x,Q^2)$ and $g_1^n(x,Q^2)$ using the relation

$$g_1^d(x,Q^2) = \frac{1}{2}\left(1 - \frac{3}{2}\omega_D\right)\left[g_1^p(x,Q^2) + g_1^n(x,Q^2)\right] , \quad (6)$$

[2] 2nd order corrections were calculated in the asymptotic range $Q^2 \gg m^2$ in Refs. [32].

where $\omega_D = 0.05 \pm 0.01$ is the D-state wave probability for the deuteron [34].

The change of the parton densities with respect to the factorization scale $\mu_f^2 = Q^2$ is described by the evolution equations, which read

$$\frac{\partial \Delta q_i^{\rm NS}(x,Q^2)}{\partial \log Q^2} = \frac{\alpha_s(Q^2)}{2\pi} \Delta P_{qq}^{NS}(x,\alpha_s) \otimes \Delta q_i^{\rm NS}(x,Q^2) \tag{7}$$

$$\frac{\partial}{\partial \log Q^2} \left(\begin{array}{c} \Delta\Sigma(x,Q^2) \\ \Delta G(x,Q^2) \end{array} \right) = \frac{\alpha_s(Q^2)}{2\pi} \Delta \boldsymbol{P}(x,\alpha_s) \otimes \left(\begin{array}{c} \Delta\Sigma(x,Q^2) \\ \Delta G(x,Q^2) \end{array} \right), \tag{8}$$

with

$$\Delta \boldsymbol{P}(x,\alpha_s) \equiv \left(\begin{array}{cc} \Delta P_{qq}(x,\alpha_s) & 2N_f \Delta P_{qg}(x,\alpha_s) \\ \Delta P_{gq}(x,\alpha_s) & \Delta P_{gg}(x,\alpha_s) \end{array} \right) . \tag{9}$$

The symbol $\otimes$ denotes the Mellin convolution

$$[A \otimes B](x) = \int_0^1 dx_1 dx_2 \delta(x - x_1 x_2) A(x_1) B(x_2) \; . \tag{10}$$

The spin–dependent coefficient functions ΔC_i^A and anomalous dimensions ΔP_{ij} are calculated to next-to-leading order in the $\overline{\rm MS}$–scheme [35–37], which we use in the present analysis. As seen from Eqs. (7) and (8), the flavor non-singlet densities Δq_i^{NS} evolve independently, while $\Delta\Sigma$ and ΔG are coupled in the evolution.

In order to solve the evolution equations, a Mellin transformation of the evolution equations Eqs. (7, 8) and the polarized parton densities Δf is being performed by calculating its Nth Mellin moment $\mathbf{M}$ as:

$$\mathbf{M}[\Delta f](N) = \int_0^1 dx \; x^{N-1} \Delta f(x) \; , N \geq N_0, N \in \mathbf{R} \; . \tag{11}$$

Here N_0 is chosen such that the integral (11) converges. Under this transformation the Mellin convolution $\otimes$ turns into an ordinary product. After the transformation has been performed the argument N is analytically continued to the complex plane. This also requires analytic continuations of harmonic sums [38], which is outlined in Refs. [39] in detail. The fundamental method of solving Eqs. (7) and (8) is described in the literature in detail, see e.g. Refs. [36,40,41].

To next-to-leading order (NLO) the solution of the flavor non–singlet and singlet evolution equations are given by

$$\Delta q_i^{\rm NS}(N,\alpha_s) = \left(\frac{\alpha_s}{\alpha_0}\right)^{-P_{\rm NS}^{(0)}/\beta_0} \left[1 - \frac{1}{\beta_0}(\alpha_s - \alpha_0)\left(P_{\rm NS}^{-(1)} - \frac{\beta_1}{\beta_0} P_{\rm NS}^{(0)}\right)\right] \Delta q_i^{\rm NS}(N,\alpha_0) \; , \tag{12}$$

$$\left(\begin{array}{c} \Delta\Sigma(N,\alpha_s) \\ \Delta G(N,\alpha_s) \end{array} \right) = \left[\mathbf{1} + \alpha_s \boldsymbol{U}_1(N)\right] \boldsymbol{L}(N,\alpha_s,\alpha_0) \left[\mathbf{1} - \alpha_0 \boldsymbol{U}_1(N)\right] \left(\begin{array}{c} \Delta\Sigma(N,\alpha_0) \\ \Delta G(N,\alpha_0) \end{array} \right) . \tag{13}$$

Here $P_{\rm NS}^{-(1)}$ denotes the NLO non-singlet $'-'$ splitting function, $\alpha_s = \alpha_s(Q^2)$ and $\alpha_0 = \alpha_s(Q_0^2)$, with Q_0^2 being the input scale. The matrices $\boldsymbol{U}_1$ and $\boldsymbol{L}$ are evolution matrices, for details see Ref. [41]. We refrain from applying so-called small x resummations [42,43], since they are very sensitive to to several series of less singular terms [41,42], which are yet unknown. Furthermore, no factorization theorem exists for these terms through which non-perturbative and perturbative contributions can be separated in a well defined way. Likewise, no other evolution equation than that governing mass singularities exists to deal with these terms.

Due to the factor–structure in Eqs. (12) and (13), the Gaussian error propagation of the input density parameters can be calculated analytically, cf. [22], for the whole Q^2 region. The covariance matrix of the parton distributions alone is completely determined by the fit to the data at the input scale.

The input distributions $\Delta q_{p,n}^{\rm NS}(N,\alpha_0)$, $\Delta\Sigma(N,\alpha_0)$ and $\Delta G(N,\alpha_0)$ are evolved to the scale Q^2. An inverse Mellin– transform to x–space is then performed by a contour integral in the complex plane around all singularities on the real axis for $x \leq x_0 \leq 1$, which can be written as

$$\Delta f(x) = \frac{1}{\pi}\int_0^\infty dz\ \mathsf{Im}\left[\exp(i\phi)x^{-c(z)}\Delta f[c(z)]\right]. \tag{14}$$

In practice an integral along the path $c(z) = c_1 + \rho[\cos(\phi) + i\sin(\phi)]$, with $c_1 = 1.1, \rho \geq 0$ and $\phi = (3/4)\pi$ is performed. The upper bound on ρ has to be chosen in accordance with the numerical convergence of the integral (14) in practice. The result $\Delta f(x)$ for the respective distribution depends on the parameters of the spin–dependent parton distributions chosen at the input scale Q_0^2, which are determined by a fit to the data and to $\Lambda_{\rm QCD}$ and $\alpha_s(M_Z^2)$, respectively.

3 Data Analysis

The QCD analysis being performed in the following is based on the spin-dependent structure functions $g_1^{p,d,n}(x,Q^2)$. These structure functions are extracted from the experimental cross section asymmetries for longitudinally polarized leptons scattered off longitudinally polarized nucleons,

$$A_{||} = \frac{\sigma^{\rightrightarrows} - \sigma^{\rightleftarrows}}{\sigma^{\rightrightarrows} + \sigma^{\rightleftarrows}}\ . \tag{15}$$

The arrows $\rightrightarrows(\rightleftarrows)$ denote parallel (anti–parallel) relative spin orientation of the incoming lepton and nucleon. The structure function ratio g_1/F_1 and the longitudinal virtual–photon asymmetry A_1 are related to $A_{||}$ by

$$\frac{g_1}{F_1} = \frac{1}{(1+\gamma^2)}\left[\frac{A_{||}}{D} + (\gamma - \eta)A_2\right] \tag{16}$$

and

$$A_1 = \frac{A_{||}}{D} - \eta A_2\ , \tag{17}$$

with

$$\frac{g_1}{F_1} = \frac{1}{(1+\gamma^2)}\left[A_1 + \gamma A_2\right]. \tag{18}$$

The asymmetry A_2 is the transverse virtual–photon asymmetry and constitutes only a small correction to g_1. Its contribution has been treated differently by various experiments as will be discussed below. The other variables are given by

$$D = \frac{1-(1-y)\epsilon}{1+\epsilon R(x,Q^2)}\ , \tag{19}$$

$$\gamma = \frac{2Mx}{\sqrt{Q^2}}\ , \tag{20}$$

$$\eta = \frac{\epsilon\gamma y}{1-\epsilon(1-y)}\ , \tag{21}$$

$$\epsilon = \frac{4(1-y)-\gamma^2y^2}{2y^2+4(1-y)+\gamma^2y^2}\ . \tag{22}$$

Here D denotes the virtual photon depolarization factor. It determines the fraction of the incoming lepton polarization transferred to the virtual photon. The variables ϵ, γ and η are kinematic factors, M denotes the mass of the nucleon and $y = (E - E')/E$ is a Bjorken scaling variable which describes the normalized energy transfer to the virtual photon, with E the incoming energy and E' the energy of the scattered lepton in the target rest frame. Finally, R denotes the ratio of the longitudinal and transverse virtual–photon absorption cross section $R(x, Q^2) = \sigma_L/\sigma_T$, which is experimentally well determined in the kinematic region considered in the present analysis.

In order to obtain $g_1(x, Q^2)$ the measured ratio g_1/F_1 has to be multiplied by the spin–independent structure function $F_1(x, Q^2)$:

$$g_1(x, Q^2) = \left(\frac{g_1}{F_1}\right)(x, Q^2) \ \times \ F_1(x, Q^2) \ . \tag{23}$$

The structure function $F_1(x, Q^2)$ can be calculated from the structure function $F_2(x, Q^2)$ by

$$F_1(x, Q^2) = \frac{(1 + \gamma^2)}{2x(1 + R(x, Q^2))} F_2(x, Q^2) \ . \tag{24}$$

For $R(x, Q^2)$ and $F_2(x, Q^2)$ parameterizations of existing measurements are available as will be discussed below.

The following data sets have been used in the present analysis: the EMC proton data [1], the E142 neutron data [2], the HERMES neutron data [3], the E154 neutron data [4, 15], the SMC proton and deuteron data [5], the E143 proton and deuteron data [6], the HERMES re-analyzed proton and the new deuteron data [7], the E155 deuteron data [8], the E155 proton data [9], the COMPASS deuteron data [11], the JLAB neutron [10], proton and deuteron data [12, 13], and the COMPASS proton data [14] [3]. The number of data points with $Q^2 \gtrsim 1.0$ GeV^2 and $W^2 \gtrsim 3.24$ GeV^2 from the different data sets are summarized in Table 1 together with the x and Q^2 ranges of the different experiments. In order to obtain the best possible statistical accuracy data on A_1, g_1/F_1 and g_1 are not averaged over the different Q^2 values measured within a certain x bin. In total 1385 data points are used. Using A_1 and g_1/F_1 data has, in addition to the higher statistics, the advantage of calculating g_1 for all these data sets in a unique way. Furthermore, g_1 data are sometimes only published as obtained from the average of asymmetries measured at different Q^2 values, while for the QCD analysis it is important to maintain the Q^2 dependence of the measured quantities.

The SLAC parameterization R_{1990} [45] is used by most of the experiments when extracting g_1. At the time of the EMC experiment this parameterization was not available yet and R was assumed to be Q^2 independent. SMC adopted a combination of R_{1990} (for $x > 0.12$) and a parameterization derived by NMC [46] (for $x < 0.12$). In the E155 experiment a recent SLAC parameterization for R, $R(1998)$ [47], was used. The changes in the data caused by using the different R–parameterizations, however, are not significant and stay within the experimental errors [4]. For all A_1 and g_1/F_1 data sets entering the present QCD analysis the SLAC $R_{1990}(x, Q^2)$ [45] and the NMC $F_2(x, Q^2)$–parameterization [48] is used to perform the calculation of g_1. The same parameterizations were used by the E154 experiment while JLAB applied the $R(1998)$ SLAC parameterization of R.

The magnitude of A_2 has been measured by SMC [49], E154 [50], E143 [6], E155x [51] and JLAB [10] and was found to be small. Its contribution to g_1/F_1 and A_1 is further suppressed by the kinematic factors γ and η and could in principle be neglected to a good approximation. On

[3] Earlier data from Ref. [44] are not considered.

[4] The EMC proton data, where the biggest impact is expected, change by a few percent only, see Ref. [18].

the other hand all the measurements have shown that the A_2 contribution can be approximated by the Wandzura–Wilczek expression [52], which is calculated from the spin-dependent structure function $g_1(x,Q^2)$ assuming that twist–2 contributions are dominant according to [5]

$$A_2(x,Q^2) = \frac{\gamma(x,Q^2)}{F_1(x,Q^2)}\Big[g_1(x,Q^2)+g_2(x,Q^2)\Big]$$

$$\stackrel{WW}{\simeq} \frac{\gamma(x,Q^2)}{F_1(x,Q^2)}\int_x^1 \frac{dz}{z} g_1(z,Q^2)\ . \tag{25}$$

The E143 experiment has exploited its measurement of A_2 at 29.1 GeV and used the Wandzura–Wilczek expression to account for A_2 for the other two lower beam energies. The measurement of A_2 by E154 and E155x was done after having published the data on A_1 and was therefore not available for a A_2 correction of A_1. While E154 neglected A_2, the E155 experiment has used the Wandzura–Wilczek approximation throughout its data. The JLAB measurement of A_2 went into the extraction of g_1^n. In HERMES the A_2 contribution to $g_1^{p,d}/F_1^{p,d}$ data has been accounted for by using a parameterization for A_2 obtained from a fit $A_2 = CM_p x/\sqrt{Q^2}$ to all available proton and deuteron data, with $C = 0.437 \pm 0.150$ for the proton and 0.246 ± 0.066 for the deuteron [7]. For all A_1 data sets used in this analysis g_1 has been calculated with the application of the Wandzura–Wilczek correction for A_2.

The data sets contain both statistical and systematic errors. It is known that the systematic errors are partly correlated, which would lead to an overestimation of the errors when added in quadrature with the statistical ones and hence to a reduction of the χ^2 value in the fitting procedure. To treat all data sets on the same footing only statistical errors were used. However, a relative normalization shift, $\mathcal{N}_i$, between the different data sets was allowed within the normalization uncertainties, $\Delta\mathcal{N}_i$, quoted by the experiments. These normalization shifts were fitted once and then fixed, see Table 1. Thereby the main systematic uncertainties coming from the measurements of the luminosity and the beam and target polarization were taken into account. The normalization shift for each data set enters as an additional term in the χ^2–expression for the fit which then reads

$$\chi^2 = \sum_{i=1}^{n^{exp}} \left[\frac{(\mathcal{N}_i - 1)^2}{(\Delta\mathcal{N}_i)^2} + \sum_{h,k=1}^{n^{data}} (\mathcal{N}_i g_{1i,h}^{data} - g_{1,h}^{theor})(\mathcal{C}_i^{-1})^{hk}(\mathcal{N}_i g_{1i,k}^{data} - g_{1,k}^{theor}) \right],$$

where the sums run over all data sets and in each data set over all data points. The covariance matrices $\mathcal{C}_i$ are diagonal for each experiment except for the case of the HERMES data [7]. The statistical errors, and consequently the covariance matrices $\mathcal{C}_i$, have been rescaled by the normalization factors $\mathcal{N}_i$. The minimization of the χ^2 value above to determine the best parameterization of the polarized parton distributions is performed using the program `MINUIT` [58] choosing a value `UP = 9.3`. Only fits giving a positive definite covariance matrix at the end have been accepted in order to be able to calculate the fully correlated 1σ statistical error bands.

4 Parameterization of the Polarized Parton Distributions

The shape chosen for the parameterization of the polarized parton distributions $\Delta f_i(x,Q^2)$

[5] Note that this relation holds also in the presence of quark and target mass corrections [16, 53, 54], for non-forward scattering [55], for diffractive scattering [56], and the gluonic contributions to heavy flavor production [57]. Related integral relations for twist–3 contributions and structure functions with electro–weak couplings were derived in Refs. [16, 54].

in x–space at the input scale Q_0^2 is :

$$x\Delta f_i(x,Q_0^2) = \eta_i A_i x^{a_i}(1-x)^{b_i}\left(1+\rho_i x^{\frac{1}{2}}+\gamma_i x\right) . \tag{26}$$

The term x^{a_i} controls the behavior of the parton density at low and $(1-x)^{b_i}$ that at large values of x, respectively. The remaining polynomial factor accounts for additional degrees of freedom at medium x.

The parameterizations are chosen to be flexible enough to describe the shape of the data and at the same time to contain not too many parameters which have to be sufficiently constrained by the available data. The choice of the shape (26) is applied in various QCD analyzes of unpolarized data, see e.g. Ref. [59].

The normalization constant A_i, being given by

$$A_i^{-1} = \left(1+\gamma_i\frac{a_i}{a_i+b_i+1}\right)B(a_i,b_i+1)++\rho_i B\left(a_i+\frac{1}{2},b_i+1\right) , \tag{27}$$

is calculated such that

$$\eta_i = \int_0^1 dx\Delta f_i(x,Q_0^2) \tag{28}$$

is the first moment of $\Delta f_i(x,Q_0^2)$ at the input scale. Here, $B(a,b)$ is the Euler Beta–function being related to the Γ–function by $B(a,b)=\Gamma(a)\Gamma(b)/\Gamma(a+b)$.

When the QCD evolution equations are solved in Mellin space as described in Section 2 a Mellin transformation of the polarized parton density $\Delta f(x,Q^2)$ is performed and a Mellin moment is calculated for complex arguments N according to

$$\begin{aligned}\mathbf{M}[\Delta f_i(x,Q_0^2)](N) &= \int_0^1 x^{N-1}dx\Delta f_i(x,Q_0^2)\\ &= \eta_i A_i\left(1+\gamma_i\frac{N-1+a_i}{N+a_i+b_i}\right)B(N-1+a_i,b_i+1)\\ &\quad +\rho_i B\left(N+a_i-\frac{1}{2},b_i+1\right) .\end{aligned} \tag{29}$$

Four spin–dependent parton densities have to be determined in the QCD analysis. They are chosen to be: $\Delta u_v(x,Q^2)$, $\Delta d_v(x,Q^2)$, $\Delta\overline{q}_s(x,Q^2)$ and $\Delta G(x,Q^2)$. As seen from Eq. (26), each spin–dependent density contains five parameters which gives a total of 20 for all four. It has been found that, in order to meet the quality of the available data and the reliability of the fitting procedure, this large number of free parameters has to be reduced, which is discussed below.

Assuming (approximate) SU(3) flavor symmetry the sea quark distribution is given by

$$\Delta\overline{q}_s(x,Q^2) = \Delta\overline{u}(x,Q^2) = \Delta\overline{d}(x,Q^2) = \Delta s(x,Q^2) = \Delta\overline{s}(x,Q^2) . \tag{30}$$

In the present analysis we refer to the inclusive polarized DIS World Data. A breaking of the flavor symmetry also for the light (sea) quarks in the polarized case is probable and has been clearly observed in the unpolarized case, cf. e.g. [30]. In the polarized case first attempts have been made to determine the individual sea quark distributions, cf. Refs. [24, 61]. We consider the evolution of the complete light polarized sea.

The first moments of the polarized valence distributions Δu_v and Δd_v, η_{u_v} and η_{d_v}, can be fixed exploiting the knowledge of the parameters F and D as measured in neutron and hyperon β–decays according to the relations:

$$\eta_{u_v} - \eta_{d_v} = F + D \,, \tag{31}$$

$$\eta_{u_v} + \eta_{d_v} = 3F - D \,. \tag{32}$$

A re–evaluation of F and D was performed on the basis of updated β–decay constants [60] leading to

$$F = 0.464 \pm 0.008 \quad \text{and} \quad D = 0.806 \pm 0.008 \tag{33}$$

and consequently to

$$\eta_{u_v} = 0.928 \pm 0.014 \quad \text{and} \quad \eta_{d_v} = -0.342 \pm 0.018 \,. \tag{34}$$

In order to compensate for the present insufficient accuracy of the data, a certain number of parameters is set to zero from the very beginning. This applies to $\rho_{u_v} = \rho_{d_v} = 0$, $\gamma_{\overline{q}_s} = \rho_{\overline{q}_s} = 0$, and $\gamma_G = \rho_G = 0$. The number of parameters to be fitted for each polarized parton density is reduced to three, i.e. to 12 in total. In addition the QCD scale $\Lambda_{\rm QCD}$ is fitted.

In the analysis it turns out that the four parameters γ_{u_v}, γ_{d_v}, $b_{\overline{q}_s}$, and b_G have very large uncertainties. The precision of the data is not high enough to constrain these parameters sufficiently. Altering them within these uncertainties does not lead to a significant change of χ^2. These four parameters were therefore fixed. The first two of them were fixed at their values obtained in the initial fitting pass, $\gamma_{u_v} = 27.64$ and $\gamma_{d_v} = 44.26$. In fixing the high–x slopes b_G and $b_{\overline{q}_s}$ a relation was adopted as derived from the unpolarized parton densities, $b_{\overline{q}_s}/b_G(\text{pol}) = b_{\overline{q}_s}/b_G(\text{unpol}) = 1.44$. Fitting with this constraint led to the following choice: $b_G = 5.61$ and $b_{\overline{q}_s} = 8.08$, see e.g. Ref. [62].

A second relation was adopted to constrain the low–x behavior of the spin–dependent gluon density with respect to the low–x behavior of the spin–dependent sea–quark distribution by $a_G = a_{\overline{q}_s} + C$ with $C = 1$. This relation, together with the relation for the high–x slopes, are suited to establish positivity for ΔG and $\Delta\overline{q}_s$. No explicit positivity constraint was assumed for Δu_v and Δd_v.

5 Determination of the Errors

5.1 Calculation of Statistical Errors

The evolved polarized parton densities and structure functions are functions of the input densities. Let $\Delta f(x, Q^2; p_i|_{i=1,k})$ be the evolved polarized density at the scale Q^2 depending on the parameters $p_i|_{i=1,k}$. Then its correlated statistical error as given by Gaussian error propagation is

$$(\sigma\Delta f)^2 = \sum_{i,j=1}^{k} \left(\frac{\partial \Delta f}{\partial p_i} \frac{\partial \Delta f}{\partial p_j} \right) \text{cov}(p_i, p_j) \,, \tag{35}$$

where $\text{cov}(p_i, p_j)$ are the elements of the covariance matrix determined in the QCD analysis. The gradients $\partial\Delta f/\partial p_i$ at the input scale Q_0^2 can be calculated analytically. Their values at Q^2 are calculated by evolution and can then be used to calculate the errors according to Eq. (35). As shown in Section 2, the covariance matrix is completely determined by the fit at the input scale

and does not change when the evolution is done in Mellin space. That means it can be used at any scale Q^2. For the expressions of the gradients at the input scale see Ref. [22].

Apart from statistical errors the data are also subject to systematic uncertainties which are even partly correlated. These correlations are not published by the experiments and can hence not be taken into account here. In the following the influence of experimental and theoretical systematic uncertainties will be investigated.

5.2 Determination of Experimental Systematic Uncertainties

The experimental systematic uncertainties were estimated from the following sources :

1. The variation of the data within their experimental systematic uncertainties.
   The procedure used to obtain the contribution from the experimental systematic uncertainties consists in shifting each data set by $\pm\sigma_{syst}$ while leaving the other data sets at their central values and looking at how much the polarized distributions change. The extreme changes from the 'central' distribution were taken as the systematic uncertainties. This was done for each of the 19 data sets used separately and, finally, the 19 contributions were added in quadrature to obtain the total contribution.

2. The variation of the data within the upper and lower limits of the NMC F_2 parameterization [48].
   When calculating $g_1(x, Q^2)$ from the asymmetry data, see Section 3, the NMC F_2–parameterization was used at its upper and lower limit to determine the changes in the polarized distributions compared to the 'central' curve. The extreme deviations from that curve were taken as the systematic uncertainties arising from the F_2 parameterization.

3. The variation of the data within the uncertainty of the R parameterization [45].
   When calculating $g_1(x, Q^2)$ from the asymmetry data, see Section 3, the SLAC R_{1990} parameterization was used at its uncertainty limits, see Ref. [45], to determine the changes in the spin–dependent distributions compared to the 'central' curve. The maximal deviations from that curve were taken as the systematic uncertainties arising from the R–parameterization.

Finally, the contributions from all three sources were added in quadrature to obtain the total contribution at each value of x, which is shown as hatched error bands in the Figures below.

5.3 Determination of Theoretical Systematic Uncertainties

The theoretical systematic uncertainties were estimated from the following sources :

1. The variation of the factorization and the renormalization scale by a factor of 2.

2. An additional variation of $\Lambda^{(4)}_{QCD}$. We varied $\Lambda^{(4)}_{QCD}$ by ± 30 MeV, which corresponds to a variation of $\alpha_s(M_Z^2)$ by ± 0.002, being a typical error in individual precision measurements, in addition to the error of $\alpha_s(M_Z^2)$ being determined in the present fit.

3. The variation of η_{u_v} and η_{d_v} within the errors of the parameters F and D, see Section 4, while keeping $g_A/g_V = F + D$ constant.

4. The variation of the parameterizations at the input scale Q_0^2.
   Two cases are considered: first, the values of the parameter ρ for Δu_v and Δd_v are added in the fit by assigning a value different from zero. Second, the values of the parameter γ for the same densities are changed compared to the values used for the central curve.

5. The variation of the standard input scale: from $Q_0^2 = 4.0$ GeV^2 to 2.0 GeV^2 and 6.0 GeV^2.

For all items always the extreme deviations from the 'central' curve were taken as the contribution to the theoretical systematic uncertainty from that source. Finally, all different contributions were added in quadrature to get the total contribution at each value of x which is shown as the second hatched error bands in the Figures below.

6 Results of the QCD Analysis

6.1 The parton distributions

In the NLO QCD fit we covered the polarized world deep-inelastic data with $Q^2 > 1$ GeV$^2, W^2 > 3.24$ GeV^2, with a value of $\chi^2/NDF = 1.12$. The parton distributions are parameterized at $Q_0^2 = 4$ GeV^2. In Table 2 the values of the fit parameters are summarized. The covariance matrix of the fit is given in Table 3. Gaussian error propagation allows to derive the error bands due to the parton densities for the various polarized observables.

In Figure 1 the polarized momentum distributions $x\Delta f_i(x)$ are presented at the scale Q_0^2. We compare with other analyzes [18–20, 24]. The $x\Delta u_v$ distribution is slightly lowered if compared to our previous analysis [22]. The most important change concerns the gluon distribution $x\Delta G$, which is lowered by about a factor of two relative to the results of Ref [22]. Comparing to the results of other analyzes the $x\Delta u_v$ turns out to be lower in a wider range, except of [24], which takes lower values from $x \sim 0.05$ on. In case of the $x\Delta d_v$-distribution all fits widely agree within the 1σ error band. This also applies for the $x\Delta\overline{q}$-distribution, with the exception of the DSSV-distribution [24], which yields smaller values of $|x\Delta\overline{q}|$. Here we have added the individual sea-quark contributions to allow for the comparison. For the polarized gluon distribution the agreement of the different fits at larger values of x agree within the 1σ error, while below $x \sim 0.02$ the fits [18–20] yield slightly higher values. The DSSV-fit [24] is located at the lower end of the error band.

In Figures 2 and 3 we analyze the systematic errors in more detail, cf. Sections 5.2 and 5.3. For the gluon distribution function $x\Delta G(x, Q_0^2)$, Figure 2, the experimental systematic errors are lower than the statistical errors, but are still significant. The combined theoretical systematic effects at NLO amount to larger values than the experimental ones. About half of the error is due to the uncertainty in $\Lambda_{\rm QCD}$. Clearly, in future analyzes based on NNLO QCD evolution this error will diminish. The effect of the experimental and theoretical systematic errors in case of the singlet distribution $x\Delta\Sigma(x, Q_0^2)$ is similar. The errors are smaller if compared to the gluon distribution. The singlet distribution at $Q_0^2 = 4$GeV^2 is negative (within the 1σ errors) for $x < 2 \cdot 10^{-2}$ and turns to positive values for $x > 4 \cdot 10^{-2}$. All the fits [18–20] lie inside the 1σ error band. In the medium x-range the DSSV distribution [24] yields somewhat larger values.

In Figure 4 we compare the fit results for the structure functions $g_1^p(x, Q^2), g_1^d(x, Q^2)$ and $g_1^n(x, Q^2)$ at $Q^2 = 5$ GeV^2 with the data, cf. Table 1, to illustrate the fit quality for the different targets as an example. Furthermore, also the results of the GRSV [19] and AAC [18] analyzes are shown. Overall a good agreement is obtained.

A further illustration of the fit quality is presented in Figure 5. Here the data for $g_1^p(x, Q^2)$ are compared to the fit including, the statistical errors. We also show the fit results of AAC, GRSV, and LSS [18–20]. Within the error bands the data agree well with the fit. In the lowest x-bins the fluctuation is somewhat larger. In some cases the EMC-data [1] lay outside the 1σ error range.

6.2 $\Lambda_{\rm QCD}$ and $\alpha_s(M_Z^2)$

The NLO QCD-analysis of the polarized world deep-inelastic data requires the fit of $\Lambda_{\rm QCD}$ along with the parameters of the non-perturbative parton distributions at the scale Q_0^2. As outlined in Table 3 the QCD-scale is correlated to all other parameters and in particular to η_G. Due to this analyzes in which $\alpha_s(M_Z^2)$ or $\Lambda_{\rm QCD}$ is imported from 3rd sources may suffer significant biases, i.e. a too *large* value of $\alpha_s(M_Z^2)(\Lambda_{\rm QCD})$ leads to a too *small* gluon distribution, aside of other effects. Despite of various precision measurements of the strong coupling constant based on theoretical NNLO (and partially even higher) precision, a thorough agreement on the value of $\alpha_s(M_Z^2)$ has not yet been reached, cf. e.g. [63]. Due to this $\Lambda_{\rm QCD}$ is determined in this analysis. We refer to $\Lambda_{\rm QCD}^{\rm NLO,(N_f=4)}$ as the NLO value for 4 active flavors. We obtain

$$\Lambda_{\rm QCD}^{(4)} = 243.5 \pm 62({\rm exp})\ \ {\rm MeV}\ . \tag{36}$$

In an earlier analysis [22] the values

$$\Lambda_{\rm QCD}^{(4)} = 235 \pm 53({\rm exp})\ \ {\rm MeV}\ \ \texttt{ISET = 3} \tag{37}$$

$$\Lambda_{\rm QCD}^{(4)} = 240 \pm 60({\rm exp})\ \ {\rm MeV}\ \ \texttt{ISET = 4} \tag{38}$$

were found, for comparison, slightly depending on some assumptions in the fit. The variation of the factorization and renormalization scales $\mu_{f,r}^2$ by a factor of 1/2 and 2, respectively, yields

$$\Lambda_{\rm QCD}^{(4)} = 243.5 \pm 62\ ({\rm exp})\ \ {}^{-37}_{+21}\ \ ({\rm FS})\ \ {}^{+46}_{-87}\ \ ({\rm RS})\ .\ {\rm MeV}\ . \tag{39}$$

Here we excluded values $\mu_{f,r}^2 < 1$ GeV^2, unlike in Ref. [22], since at scales lower than 1 GeV^2 the perturbative description cannot be considered reliable anymore.

Correspondingly, for $\alpha_s(M_Z^2)$ one obtains

$$\alpha_s(M_Z^2) = 0.1132\ \ {}^{+0.0043}_{-0.0051}\ \ ({\rm exp})\ \ {}^{-0.0029}_{+0.0015}\ \ ({\rm FS})\ \ {}^{+0.0032}_{-0.0075}\ \ ({\rm RS})\ , \tag{40}$$

with combined errors of

$$\alpha_s(M_Z^2) = 0.1132\ \ {}^{+0.0056}_{-0.0095}\ \ . \tag{41}$$

Due to the NLO analysis the factorization- and renormalization scale uncertainties are still dominant. The values are well compatible with recent determinations of the strong coupling constant at NNLO and N^{3}LO from deep-inelastic data :

$$\alpha_s(M_Z^2) = 0.1134\ {}^{+0.0019}_{-0.0021}\quad {\rm NNLO}\quad [27] \tag{42}$$

$$\alpha_s(M_Z^2) = 0.1141\ {}^{+0.0020}_{-0.0022}\quad {\rm N^3LO}\quad [27] \tag{43}$$

$$\alpha_s(M_Z^2) = 0.1135 \pm 0.0014\quad {\rm NNLO,\ FFS}\quad [30] \tag{44}$$

$$\alpha_s(M_Z^2) = 0.1129 \pm 0.0014\quad {\rm NNLO,\ BSMN}\quad [30] \tag{45}$$

$$\alpha_s(M_Z^2) = 0.1124 \pm 0.0020\quad {\rm NNLO,\ dyn.\ approach}\quad [28] \tag{46}$$

$$\alpha_s(M_Z^2) = 0.1158 \pm 0.0035\quad {\rm NNLO,\ stand.\ approach}\quad [28] \tag{47}$$

$$\alpha_s(M_Z^2) = 0.1171 \pm 0.0014\quad {\rm NNLO}\quad [29] \tag{48}$$

More recent unpolarized NNLO fits, including the combined HERA data [64], yield

$$\alpha_s(M_Z^2) = 0.1147 \pm 0.0012 \quad \text{NNLO} \quad [65] \tag{49}$$

$$\alpha_s(M_Z^2) = 0.1145 \pm 0.0042 \quad \text{NNLO, (preliminary)} \quad [66] \tag{50}$$

The central value of the present fit (41) does well compare with the above values. They are located below the present weighted average of $\alpha_s(M_Z^2)$ measurements [63] of

$$\alpha_s(M_Z^2) = 0.1184 \pm 0.0007 \; . \tag{51}$$

The error given in (51) does not include the relative systematics of the different classes of measurements.

We would like to mention that recent determinations of $\alpha_s(M_Z^2)$ using event shape moments for high energy e^+e^- annihilation data from PETRA and LEP including power corrections the following values were obtained :

$$\alpha_s(M_Z^2) = 0.1135 \pm 0.0002\ (\text{exp}) \pm 0.005\ (\Omega_1) \pm 0.0009\ (\text{pert}) \quad \text{NNLO} \quad [67] \tag{52}$$

$$\alpha_s(M_Z^2) = 0.1153 \pm 0.0017\ (\text{exp}) \pm 0.0023\ (\text{th}) \quad \text{NNLO} \quad [68] \tag{53}$$

Also these measurements of $\alpha_s(M_Z^2)$ yield low values. They show that the results obtained analyzing deep–inelastic data do not form a special case. The systematics of the different extractions of $\alpha_s(M_Z^2)$ has to be understood in more detail in the future.

Fit results from previous polarized analyzes like [15, 17, 25] were summarized in [22]. In Figure 6 we compare recent determinations at NNLO and N^{3}LO for unpolarized and at NLO for prolarized deep-inelastic scattering.

6.3 Moments of Polarized Parton Distributions

We calculate the lowest moments of the polarized parton densities

$$\langle f(x) \rangle_n = \int_0^1 dx x^n \Delta f(x) \; , \tag{54}$$

where $\Delta f(x)$ denote the different polarized (number) density distributions. The moments $n = 0, ..., 3$ are given in Table 4. The behaviour of these distributions outside the kinematic range in which the fit is performed bear uncertainties, which are difficult to predict for theses non-perturbative quantities. [6] Instead of presenting necessarily uncertain models for this range, we compute the respective part of the moments for values $x < 0.005$ and $x > 0.75$ extrapolating the present distributions to the range $x \in [0, 1]$.

The zeroth moments of the polarized quark- and gluon distributions as well as the contributions due to the quark- and gluon angular momenta, L_q and L_g, constitute the nucleon spin

$$\frac{1}{2} = \frac{1}{2}\langle \Delta\Sigma(x) \rangle_0 + \langle \Delta G(x) \rangle_0 + L_q + L_g \; . \tag{55}$$

We obtain

$$\langle \Delta\Sigma(x, Q_0^2) \rangle_0 = 0.216 \pm 0.079 \tag{56}$$

$$\langle \Delta G(x, Q_0^2) \rangle_0 = 0.462 \pm 0.430 \; , \tag{57}$$

[6] We remind the failure in predicting the lower x behaviour of the structure function $F_2(x, Q^2)$ prior the HERA measurements until 1992, which assumed a slightly falling or constant behaviour below $x \simeq 10^{-2}$, whereas a strong rise was measured at HERA.

at $Q_0^2 = 4\text{GeV}^2$. For Eq. (55) this yields

$$\frac{1}{2} = (0.570 \pm 0.437) + L_q + L_g \ . \tag{58}$$

The error of ΔG is clearly dominant.

The results given in Table 4 can be compared to ab initio calculations of these moments in Lattice Gauge Theory. There we also compare with the values obtained in our previous analysis [22]. In the present analysis the first moments ($n = 0$) of the polarized valence quark distributions are determined by the values of F and D and are fixed in the fit. Comparing to the results of [22], `ISET = 3` [7] slightly larger values are obtained for the moments of $\Delta u_v(x, Q^2)$ and slightly lower values for $\Delta d_v(x, Q^2)$ and $\Delta\overline{q}(x, Q^2)$. A very significant change is obtained for the moments of the polarized gluon density, where the moments reduced by a factor of about two comparing to [22]. Although being positive, the latter moments are now compatible with zero in the 1σ errors.

First lattice results for the moments $n = 0, 1, 2$ of the polarized quark distributions were given about ten years ago. Meanwhile many systematic effects in the simulation have been improved further. Still there are differences in the different simulations. Rather aiming on a detailed comparison with the values in Table 4 we give a brief summary of the current status. A recent survey has been given in [69]. Lattice results on $\langle \Delta u - \Delta d \rangle_0$ for $m_\pi^2 = 0.029...0.48\text{GeV}^2$ were given in [70–73] by the BGR, RBC, LHPC, ETMC, QCDSF-collaborations using dynamical quarks. Most of the values are yet below the experimental value. The QCDSF collaboration [73] performed simulations at $m_\pi = 170\,\text{MeV}$ and obtained

$$\langle \Delta u(x) - \Delta d(x) \rangle_0 = 1.17 \pm 0.05 \ , \tag{59}$$

$$\frac{\langle \Delta u(x) - \Delta d(x) \rangle_0}{\langle \Delta u(x) + \Delta d(x) \rangle_0} = 0.47 \pm 0.02 \ . \tag{60}$$

For the first moment the following values were determined

$$\langle \Delta u - \Delta d \rangle_1 = 0.271 \pm 0.040, \qquad m_\pi = 493\,\text{MeV}, \qquad [70] \tag{61}$$

$$= 0.252 \pm 0.020, \qquad m_\pi = 352\,\text{MeV}, \qquad [72] \tag{62}$$

which are larger than the value

$$\langle \Delta u - \Delta d \rangle_1 = 0.190 \pm 0.008 \tag{63}$$

determined in the present analysis.

Results on the second moment were given in [70]

$$\langle \Delta u - \Delta d \rangle_2 = 0.083 \pm 0.012, \qquad m_\pi = 493\,\text{MeV}, \tag{64}$$

$$\tag{65}$$

to be compared to

$$\langle \Delta u - \Delta d \rangle_2 = 0.063 \pm 0.004 \tag{66}$$

obtained in this analysis.

Results of older lattice simulations [74] were discussed in [22] previously. The values given above for the 1st and 2nd moment are based on theoretically much improved simulations, if compared to early investigations [74]. Yet, the moments obtained yield similar values. Comparing the lattice results with the results obtained in QCD-fits to the polarized deep-inelastic world data one observes a similar trend of values but not yet agreement.

[7] The NLO results for `ISET = 4` are quite similar.

7 Higher Twist

So far we have applied the twist-2 approximation at NLO to describe the spin–dependent structure function g_1. As the data may contain contributions from higher twist (HT) it is of interest to look for possible effects of such contributions. A thorough description of higher twist anomalous dimensions and Wilson coefficients to NLO is still missing, even for the twist–4 contributions. Therefore we will perform a purely phenomenological analysis. Similar to the approach of Ref. [75] for the structure function F_2, where a higher twist term is parameterized by the ansatz

$$h_{HT}(x,Q^2) = \frac{C_i(x)}{Q^2}, \tag{67}$$

used multiplicative to the leading twist (LT) contribution, $g_1(x,Q^2)$ is described by

$$g_1^{HT}(x,Q^2) = g_1^{LT}(x,Q^2)\left[1 + h_{HT}(x,Q^2)\right]. \tag{68}$$

This approach has to be handled with great care, since the coefficients $C_i(x)$ are actually also Q^2 dependent. They consist of a combination of various terms which exhibit different scaling violations. The relation to $\Lambda_{\rm QCD}$ is completely masked here. Moreover, higher twist contributions should have a flavor-dependence and are not expected to be the same in case of polarized and unpolarized deep-inelastic scattering.

The kinematic x–range being covered by experiment is divided into 5 bins and the coefficient $C_i(x)$ has to be determined in each bin and for each target. The resulting coefficients for the proton and the deuteron target, $C_i^p(x)$ and $C_i^d(x)$, are summarized in Table 5. The coefficient $C_i^n(x)$ is calculated from $C_i^p(x)$ and $C_i^d(x)$ by the relation

$$C_i^n(x) = \frac{2}{1-1.5\omega_D} C_i^d(x) - C_i^p(x)\ . \tag{69}$$

with $\omega_D = 0.05 \pm 0.01$ [34]. All three coefficients are compatible with zero within their errors as can be seen from Figure 7 where they are shown as a function of x. Therefore, the present data do not contain significant higher twist contributions in the range $Q^2 > 1$ GeV^2 and a NLO QCD analysis can be carried out in the leading twist approximation. This result is in disagreement to Ref. [21]. Note that in the latter analysis a partonic description of $F_1(x,Q^2)$ down to low values of Q^2 is used, while we refer to the measured function. Unlike the case for the large x valence quark region, in which dynamical higher twist terms are extracted consistently in the unpolarized case, cf. Refs. [27, 76, 77], the situation is more involved for the low x-region. The dynamics is clearly different in both these domains due to the contributing parton species. As has been shown in [78], different power corrections cancel each other in the small x region.

8 Conclusions

A QCD analysis of the polarized deep-inelastic world data has been performed at NLO, including the effects of charm production to first order. We derived a parameterization for the polarized parton distributions and $\Lambda_{\rm QCD}^{N_f=4}$ with the error correlations between the fitted parameters applying the χ^2–method. Detailed comparisons have been performed with recent parameterizations [18–20, 24]. The present data are not accurate enough to determine all the shape parameters at a sufficient accuracy. Due to this some of the parameters have to be fixed after an initial phase of the analysis to a model-value. If compared to our previous analysis [22] the more recent data

lead to a smaller gluon distribution which is for a wide region of x compatible with zero within the 1σ error. We determined both the experimental and theoretical systematic effects. Both the central values of the parton densities and their 1σ error are made available in form of a numerical parameterization in the range $x \in [10^{-9}, 1]$, $Q^2 \in [1, 10^6]$ GeV^2. These distributions can be used for polarized hard–scattering processes at hadron– and lepton–nucleon colliders for various observables, including error propagation w.r.t. the accuracy of the parton densities. The implementation in terms of grid-interpolation is well suited also for Monte Carlo simulations.

The QCD-scale was determined by $\Lambda_{\rm QCD}^{N_f=4} = 243.5 \pm 62\ ({\rm exp})\ {}^{+59}_{-90}\ ({\rm th})$ MeV, corresponding to $\alpha_s^{\rm NLO}(M_Z^2) = 0.1132\ {}^{+0.0056}_{-0.0095}$. The central value is well compatible with other measurements, cf. [27, 28, 30, 65–68]. The errors are still rather large, also because of the scale variation uncertainties at NLO. Nonetheless the correlated determination of $\alpha_s(M_Z^2)$ with the parton densities is of importance to avoid biases in particular w.r.t. to the size of the gluon distribution function.

We also determined potential higher twist contributions, which were found to be compatible with zero in the whole kinematic range within the present errors. Based on the results of the present analysis we computed the lowest moments of the individual twist–2 parton densities. For the lowest moment $(1/2)\langle\Delta\Sigma(x)\rangle_0 + \langle\Delta G(x)\rangle_0$ we obtain 0.570 ± 0.437 at $Q_0^2 = 4$ GeV^2, which is well compatible with the nucleon spin $1/2$ even without angular momentum contributions. However, the error is dominated by that of the polarized gluon distribution. The moments may be be compared to upcoming lattice simulations based on dynamical quarks of the corresponding operator matrix elements. The present results are not yet in agreement, although the tendency of values is visible. Runs at even smaller values of m_π seem to be necessary.

Acknowledgment. We would like to thank S. Alekhin, E. Aschenauer, L. Di Nardo, M. Göckeler, K. Jansen, W.D. Nowak, D. Renner, and G. Schierholz for discussions. This work was supported in part by DFG Sonderforschungsbereich Transregio 9, Computergestützte Theoretische Teilchenphysik and the European Commission MRTN HEPTOOLS under Contract No. MRTN-CT-2006-035505.

9 Appendix: The FORTRAN-code for the parton densities and their errors

A fast FORTRAN program is available to represent the polarized parton densities $x\Delta u_v(x,Q^2)$, $x\Delta d_v(x,Q^2)$, $x\Delta G(x,Q^2)$, and $x\Delta\bar{q}(x,Q^2)$, as well as the polarized structure functions $xg_1^p(x,Q^2)$ and $xg_1^n(x,Q^2)$ at NLO in the $\overline{\rm MS}$–scheme together with the parameterizations of their 1σ errors. The following ranges in x and Q^2 are covered:

$$10^{-9} < x < 1 \quad , \quad 1\ \mathrm{GeV}^2 < Q^2 < 10^6\ \mathrm{GeV}^2.$$

The polarized distributions are the result of a fit to the world data on spin asymmetries, i.e. $A_1^{p,n,d}$ or $g_1/F_1^{p,n,d}$, as described above. The SUBROUTINE PPDF returns the values of the polarized distributions, always multiplied by x, at a given point in x and Q^2 by interpolating the data on specified grids. The interpolation in x is done by cubic splines and in Q^2 by a linear interpolation in $\log(Q^2)$. [8]

The parton distributions are evaluated by

```
SUBROUTINE POLPDF(ISET, X, Q2, UV, DUV, DV, DDV, GL, DGL, SEA, DSEA,
                  G1P,DG1P,G1N,DG1N),
```

with ISET = 1. All non-integer variables are of the type REAL*8. The calling routine has to contain the COMMON/INTINI/ IINI. Before the first call to SUBROUTINE POLPDF the initialization is set by IINI = 0.

The parameters X, Q^2 [GeV^2] are x and Q^2. The momentum densities of the polarized up- and down valence quarks, gluons and the sea quarks are UV, DV, GL, SEA, with SEA $= x\Delta u_s = x\Delta d_s = x\Delta\overline{u} = x\Delta\overline{d} = x\Delta s = x\Delta\overline{s}$. Correspondingly, DUV is the 1σ error of UV etc. and G1P and G1N are the values of the electromagnetic structure functions xg_1^p and xg_1^n.

The programme example.f reads the data-grid qcd_nlo_905_0.grid and is compiled using gfortran at a LINUX-system. The test-code produces the test-output for the structure-functions xg1p, xg1n, xg1d and their 1σ errors dxg1p, dxg1n, dxg1d :

```
* x,Q2,xg1p,dxg1p,xg1n,dxg1n,xg1d,dxg1d
  0.100000  4.000000  0.027295  0.001559 -0.010928  0.001479  0.007570  0.000994
  0.200000  4.000000  0.044602  0.001396 -0.009622  0.001895  0.016178  0.001088
  0.300000  4.000000  0.053325  0.001135 -0.004909  0.001934  0.022392  0.001037
  0.400000  4.000000  0.052437  0.001132 -0.000395  0.002209  0.024069  0.001148
  0.500000  4.000000  0.043976  0.001371  0.002429  0.002272  0.021462  0.001227
  0.600000  4.000000  0.032110  0.001822  0.003287  0.001921  0.016371  0.001224
  0.700000  4.000000  0.018456  0.001858  0.002643  0.001254  0.009759  0.001037
  0.800000  4.000000  0.007465  0.001254  0.001340  0.000557  0.004072  0.000634
  0.900000  4.000000  0.001337  0.000383  0.000284  0.000115  0.000750  0.000185
  0.950000  4.000000  0.000215  0.000087  0.000049  0.000023  0.000122  0.000042
```

The program can be received on request via e-mail to Johannes.Bluemlein@desy.de or Helmut.Boettcher@desy.de or from http://www-zeuthen.desy.de/~blumlein.

[8] We thank S. Kumano and M. Miyama of the AAC–collaboration for allowing us to use their interpolation routines.

10 Tables

Experiment	x–range	Q^2–range $[GeV^2]$	data points type	data points #	$\mathcal{N}_i$
E143(p) [6]	0.027 – 0.749	1.17 – 9.52	g_1/F_1	82	0.963
HERMES(p) [7]	0.026 – 0.731	1.12 – 14.29	A_1	37	0.970
E155(p) [9]	0.015 – 0.750	1.22 – 34.72	g_1/F_1	24	1.003
SMC(p) [5]	0.004 – 0.484	1.14 – 72.10	A_1	59	0.960
EMC(p) [1]	0.015 – 0.466	3.50 – 29.5	A_1	10	0.964
CLAS1(p) [12]	0.125 – 0.575	1.10 – 4.16	A_1	10	1.010
CLAS2(p) [13]	0.292 – 0.592	1.01 – 4.96	g_1/F_1	191	1.030
COMPASS(p) [14]	0.005 – 0.568	1.10 – 62.10	A_1	15	0.955
proton				428	
E143(d) [6]	0.027 – 0.749	1.17 – 9.52	g_1/F_1	82	0.960
HERMES(d) [7]	0.026 – 0.731	1.12 – 14.29	A_1	37	0.970
E155(d) [8]	0.015 – 0.750	1.22 – 34.79	g_1/F_1	24	0.979
SMC(d) [5]	0.004 – 0.483	1.14 – 71.76	A_1	65	0.998
COMPASS(d) [11]	0.005 – 0.566	1.10 – 55.30	A_1	15	0.952
CLAS1(d) [12]	0.125 – 0.575	1.01 – 4.16	A_1	10	1.003
CLAS2(d) [13]	0.298 – 0.636	1.01 – 4.16	g_1/F_1	662	1.014
deuteron				895	
E142(n) [2]	0.035 – 0.466	1.10 – 5.50	A_1	33	0.989
HERMES(n) [3]	0.033 – 0.464	1.22 – 5.25	g_1	9	0.970
E154(n) [4]/ [15]	0.017 – 0.564	1.20 – 15.00	g_1	17	0.980
JLAB(n) [10]	0.330 – 0.600	2.71 – 4.83	g_1	3	1.000
neutron				62	
total				1385	

Table 1: Number of data points on A_1, g_1/F_1 or g_1 for $Q^2 > 1.0$ GeV^2 and $W^2 > 3.24$ GeV^2 used in the present QCD analysis. For each experiment are given the x and Q^2 ranges, the type of quantity measured, the number of data points for each given target, and the fitted normalization shifts $\mathcal{N}_i$ (see text).

Δu_v	η	0.928 (fixed)	$\Delta\bar{q}_s$	η	-0.417 $\pm$ 0.079
	a	0.239 $\pm$ 0.027		a	0.365 $\pm$ 0.164
	b	3.031 $\pm$ 0.178		b	8.080 (fixed)
	ρ	0.0 (fixed)		ρ	0.0 (fixed)
	γ	27.64 (fixed)		γ	0.0 (fixed)
Δd_v	η	-0.342 (fixed)	ΔG	η	0.461 $\pm$ 0.430
	a	0.128 $\pm$ 0.068		a	$a_{\Delta\bar{q}_s} + 1$
	b	4.055 $\pm$ 0.879		b	5.610 (fixed)
	ρ	0.0 (fixed)		ρ	0.0 (fixed)
	γ	44.26 (fixed)		γ	0.0 (fixed)
$\Lambda^{(4)}_{QCD} = 243 \pm 62$ MeV			$\chi^2/NDF = 1537/1377 = 1.12$		

Table 2: Final parameter values and their statistical errors at the input scale $Q_0^2 = 4.0$ GeV^2.

	$\Lambda^{(4)}_{QCD}$	a_{u_v}	b_{u_v}	a_{d_v}	b_{d_v}	η_{sea}	a_{sea}	η_G
$\Lambda^{(4)}_{QCD}$	**3.85E-3**							
a_{u_v}	-4.08E-4	**7.55E-4**						
b_{u_v}	-1.14E-3	4.30E-3	**3.18E-2**					
a_{d_v}	2.75E-3	-9.39E-4	-4.44E-3	**4.61E-3**				
b_{d_v}	2.38E-2	-8.34E-3	-1.03E-2	4.51E-2	**7.73E-1**			
η_{sea}	1.79E-3	-7.20E-4	-3.79E-3	2.38E-3	2.23E-2	**6.32E-3**		
a_{sea}	-5.65E-3	3.04E-3	1.65E-2	-8.26E-3	-7.39E-2	8.07E-4	**2.70E-2**	
η_G	-1.96E-2	8.32E-3	4.25E-2	-2.16E-2	-1.68E-1	-2.21E-2	4.17E-2	**1.85E-1**

Table 3: The covariance matrix for the $7+1$ parameter NLO fit based on the world asymmetry data.

Distribution	n	Fit Results		[22], set 3
		value	value out of range	
Δu_v	0	0.928 ± 0.000	$0.158 \vert 3.3\text{E}{-3}$	0.926 ± 0.071
	1	0.153 ± 0.004	$1.6\text{E}{-4} \vert 2.7\text{E}{-3}$	0.163 ± 0.014
	2	0.052 ± 0.002	$0 \vert 2.1\text{E}{-3}$	0.055 ± 0.006
	3	0.023 ± 0.001	$0 \vert 1.7\text{E}{-3}$	0.024 ± 0.003
Δd_v	0	-0.342 ± 0.000	$-0.110 \vert -2.1\text{E}{-4}$	-0.341 ± 0.123
	1	-0.037 ± 0.007	$-7.0\text{E}{-5} \vert -1.7\text{E}{-4}$	-0047 ± 0.021
	2	-0.010 ± 0.002	$0 \vert -1.3\text{E}{-4}$	-0.015 ± 0.009
	3	-0.004 ± 0.001	$0 \vert -1.1\text{E}{-4}$	-0.006 ± 0.005
Δu–Δd	0	1.270 ± 0.000	$0.267 \vert 3.5\text{E}{-3}$	1.267 ± 0.142
	1	0.190 ± 0.008	$2.3\text{E}{-4} \vert 2.8\text{E}{-3}$	0.210 ± 0.025
	2	0.063 ± 0.004	$0 \vert 2.3\text{E}{-3}$	0.070 ± 0.011
	3	0.027 ± 0.002	$0 \vert 1.8\text{E}{-3}$	0.030 ± 0.006
Δu	0	$0.866 \pm 2\text{E}{-5}$	$0.136 \vert 3.3\text{E}{-3}$	0.851 ± 0.075
	1	0.151 ± 0.004	$1.3\text{E}{-4} \vert 2.7\text{E}{-3}$	0.160 ± 0.014
	2	0.052 ± 0.002	$0 \vert 2.1\text{E}{-3}$	0.055 ± 0.006
	3	0.023 ± 0.001	$0 \vert 1.7\text{E}{-3}$	0.024 ± 0.003
Δd	0	$-0.404 \pm 3\text{E}{-5}$	$-0.132 \vert -2.1\text{E}{-4}$	-0.415 ± 0.124
	1	-0.039 ± 0.007	$-1.0\text{E}{-4} \vert -1.7\text{E}{-4}$	-0.050 ± 0.022
	2	-0.011 ± 0.002	$-0 \vert -1.3\text{E}{-4}$	-0.015 ± 0.009
	3	-0.004 ± 0.001	$0 \vert -1.1\text{E}{-4}$	-0.006 ± 0.005
$\Delta\overline{q}$	0	-0.062 ± 0.013	$-0.02 \vert 0$	-0.074 ± 0.017
	1	$-2.5\text{E}{-3} \pm 1.2\text{E}{-3}$	$-3.0\text{E}{-5} \vert 0$	-0.003 ± 0.001
	2	$-3.3\text{E}{-4} \pm 2.0\text{E}{-4}$	$0 \vert 0$	$-4.0\text{E}{-4} \pm 1.0\text{E}{-4}$
	3	$-7.0\text{E}{-5} \pm 4.0\text{E}{-5}$	$0 \vert 0$	$-8.0\text{E}{-5} \pm 2.0\text{E}{-5}$
ΔG	0	0.462 ± 0.430	$0.004 \vert 1.0\text{E}{-4}$	1.062 ± 0.549
	1	0.079 ± 0.079	$1.0\text{E}{-5} \vert 8.0\text{E}{-5}$	0.184 ± 0.103
	2	0.021 ± 0.021	$0 \vert 6.3\text{E}{-5}$	0.050 ± 0.028
	3	0.007 ± 0.007	$0 \vert 4.9\text{E}{-5}$	0.017 ± 0.010

Table 4: Moments of the NLO parton densities and their combinations for the present analysis at $Q^2 = 4\ \text{GeV}^2$. The value of the respective moment integrating only outside the x–range in which currently deep–inelastic scattering data are measured, $0.005 < x < 0.75$, are given for comparison (lower|upper part). The errors are the 1σ correlated errors.

$< x >$	$C_i^p, [\mathrm{GeV}^2]$	$C_i^d, [\mathrm{GeV}^2]$
0.060	-0.020 $\pm$ 0.089	0.030 $\pm$ 0.131
0.150	-0.010 $\pm$ 0.036	0.140 $\pm$ 0.082
0.275	-0.041 $\pm$ 0.027	-0.005 $\pm$ 0.054
0.425	-0.068 $\pm$ 0.055	0.007 $\pm$ 0.059
0.625	0.124 $\pm$ 0.172	0.008 $\pm$ 0.114

Table 5: The higher twist coefficients $C_i^p(x)$ and $C_i^d(x)$ as a function of x.

11 Figures

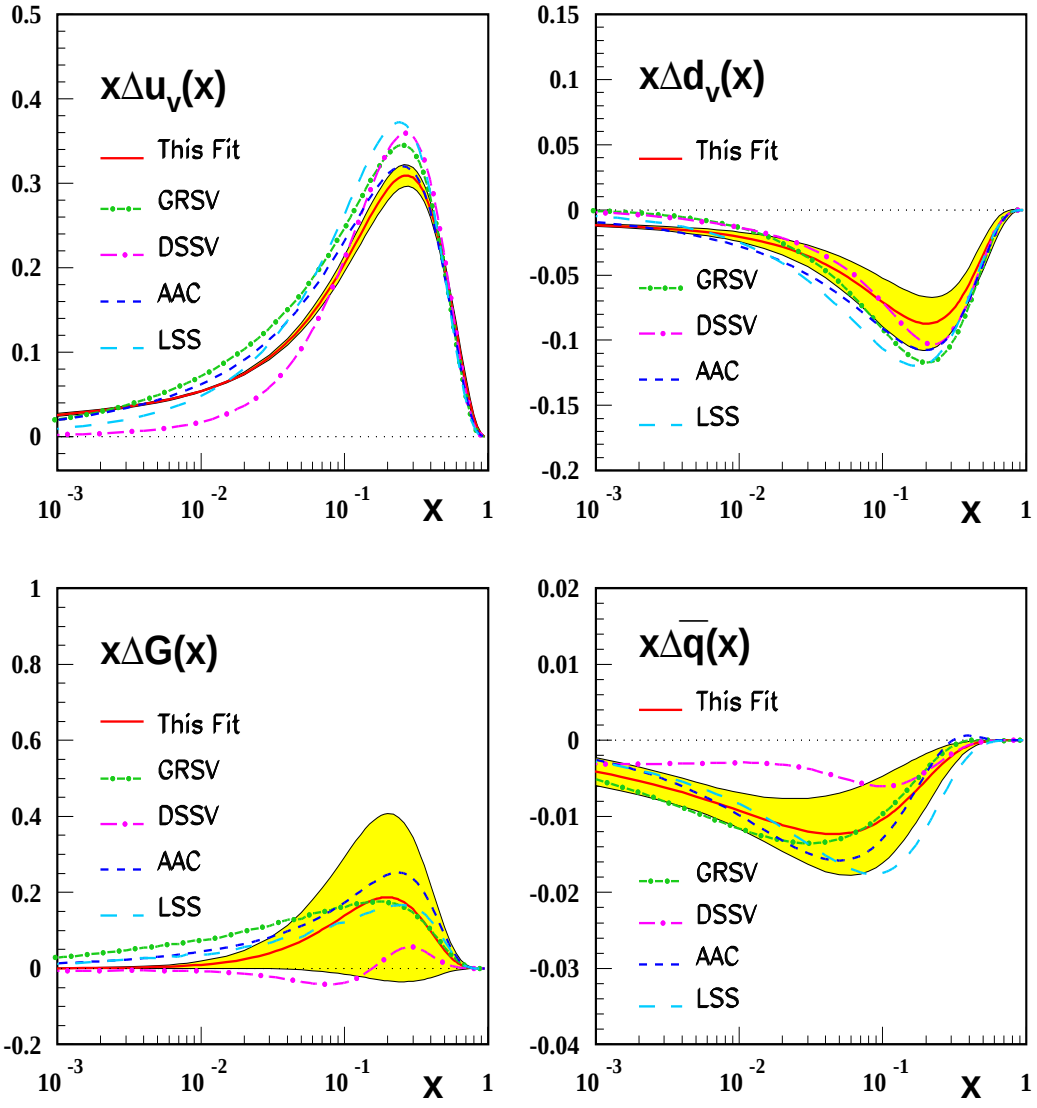

Figure 1: NLO polarized parton distributions at the input scale $Q_0^2 = 4.0$ GeV^2 (solid line) compared to results obtained by GRSV (dashed–dotted line) [19], DSSV (long dashed–dotted line) [24], AAC (dashed line) [18], and LSS (long dashed line) [20]. The shaded areas represent the fully correlated 1σ error bands calculated by Gaussian error propagation.

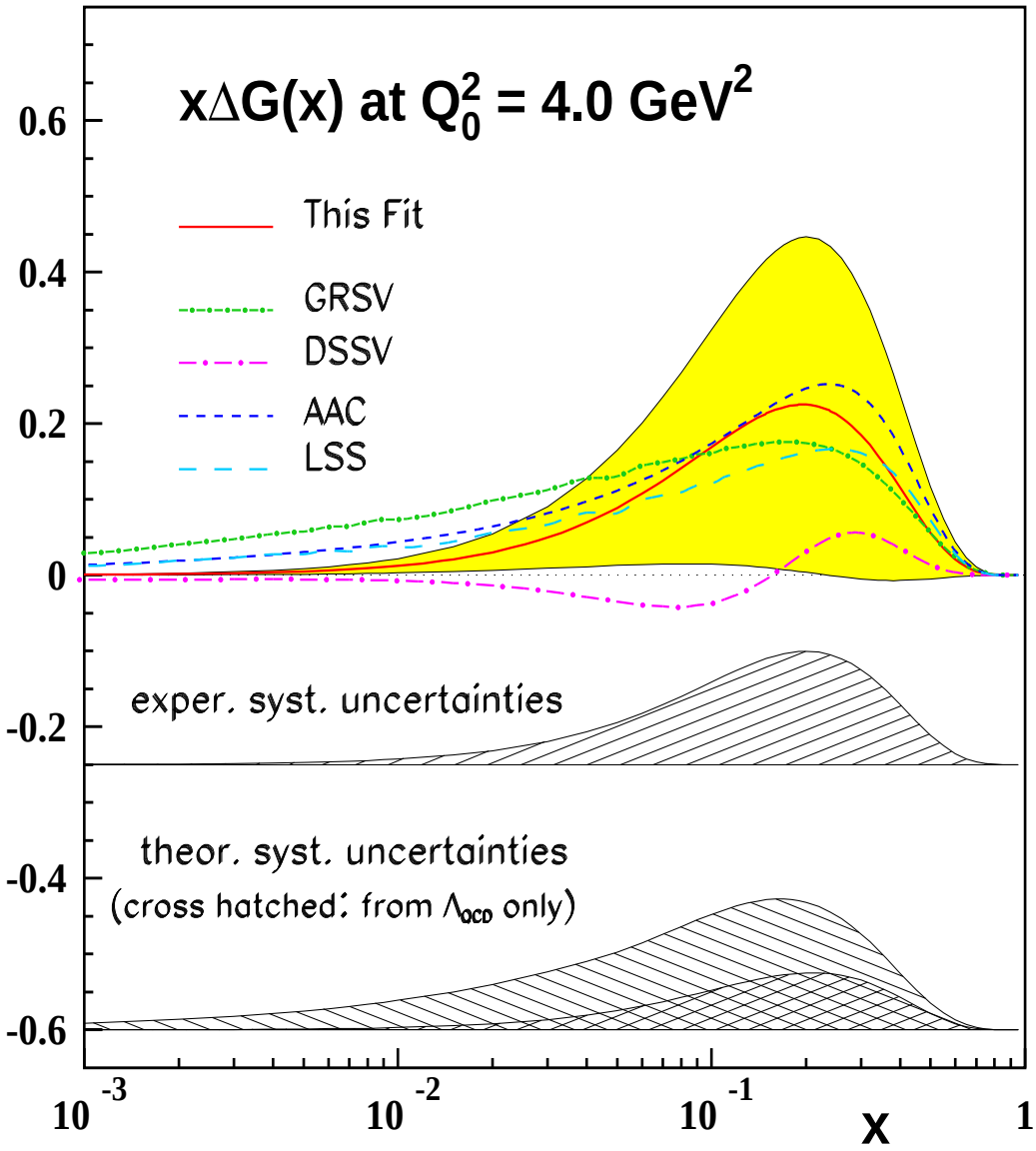

Figure 2: The polarized parton density $x\Delta G(x)$ at $Q_0^2 = 4.0$ GeV^2 as a function of x (solid line). The shaded area is the fully correlated 1σ statistical error band and the hatched areas are the systematic uncertainties. Results from GRSV (dashed–dotted line) [19], DSSV (long dashed–dotted line) [24], AAC (dashed line) [18], and LSS (long dashed line) [20] are shown for comparison.

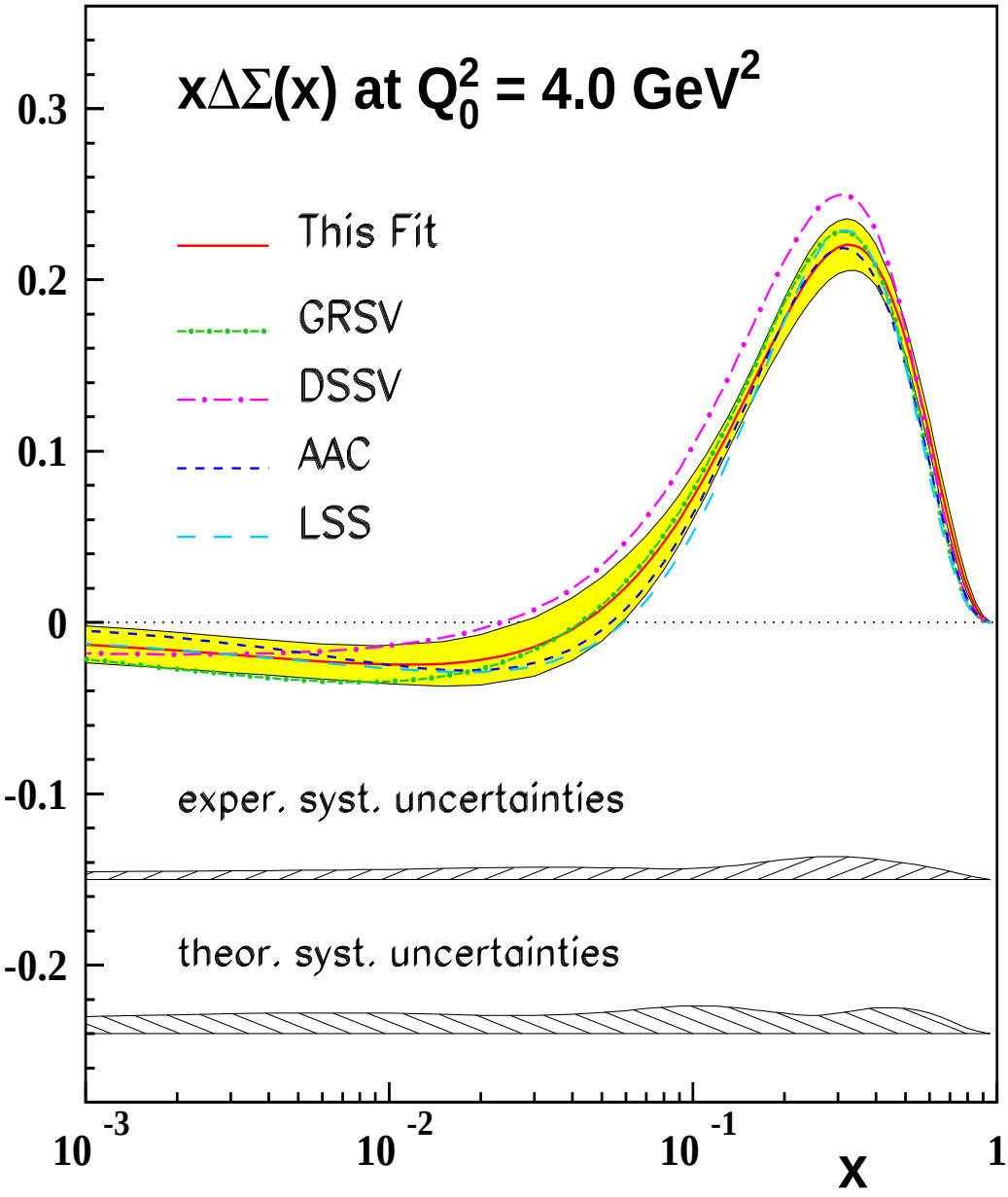

Figure 3: The polarized parton density $x\Delta\Sigma(x)$ at $Q_0^2 = 4.0$ GeV^2 as a function of x (solid line). The shaded area is the fully correlated 1σ statistical error band and the hatched areas are the systematic uncertainties. Results from GRSV (dashed–dotted line) [19], DSSV (long dashed–dotted line) [24], AAC (dashed line) [18], and LSS (long dashed line) [20] are shown for comparison.

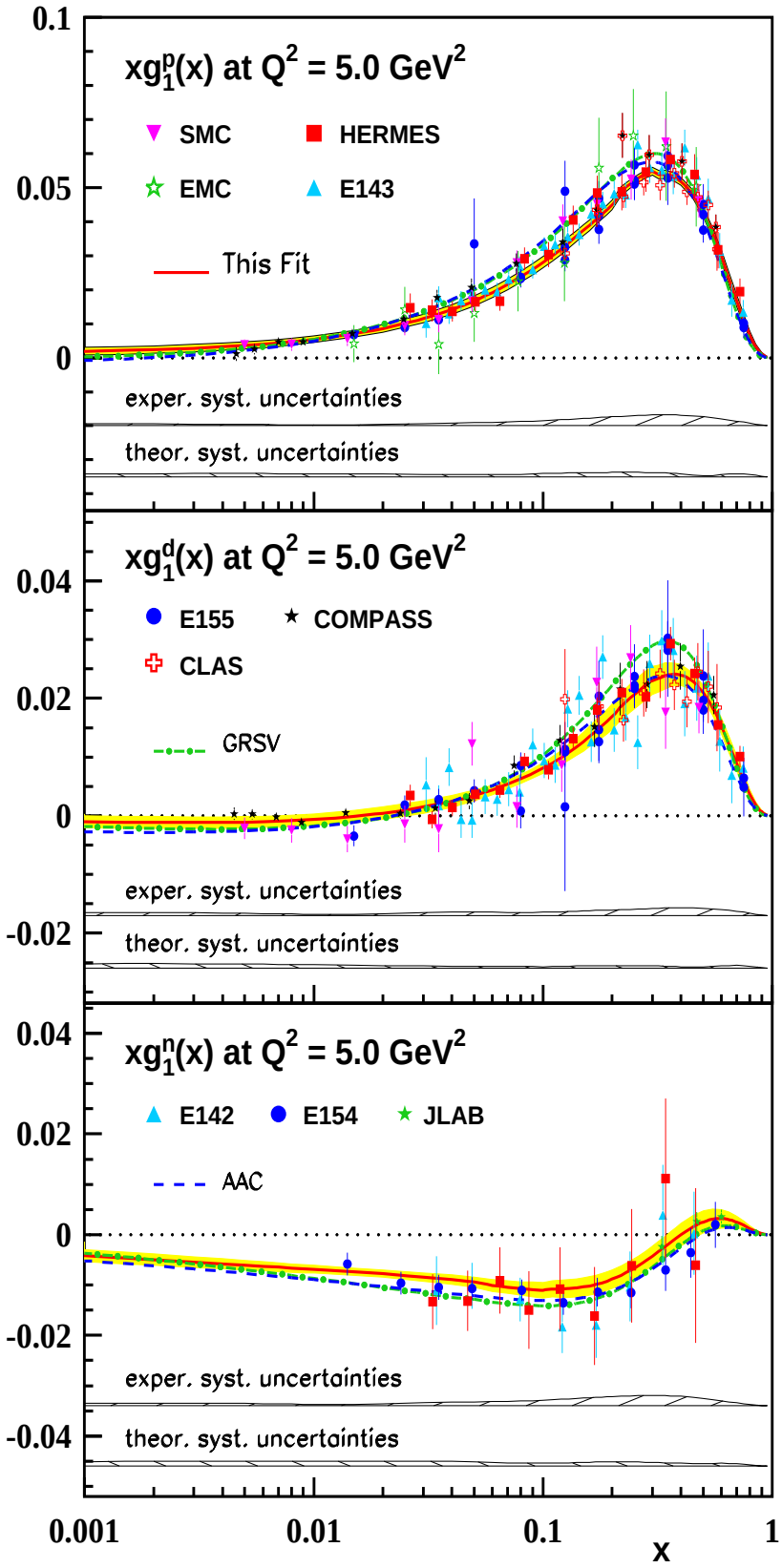

Figure 4: The spin–dependent structure functions $xg_1^p(x)$, $xg_1^d(x)$ and $xg_1^n(x)$ as a function of x. The experimental data are evolved to a common value of $Q^2 = 5$ GeV^2. The error bars shown are the statistical and systematic ones added in quadrature. The experimental distributions are well described (solid curve) within the statistical (shaded areas) and systematic (hatched areas) error bands. The curves obtained by GRSV (dashed-dotted) [19] and AAC (dashed) [18] are shown for comparison.

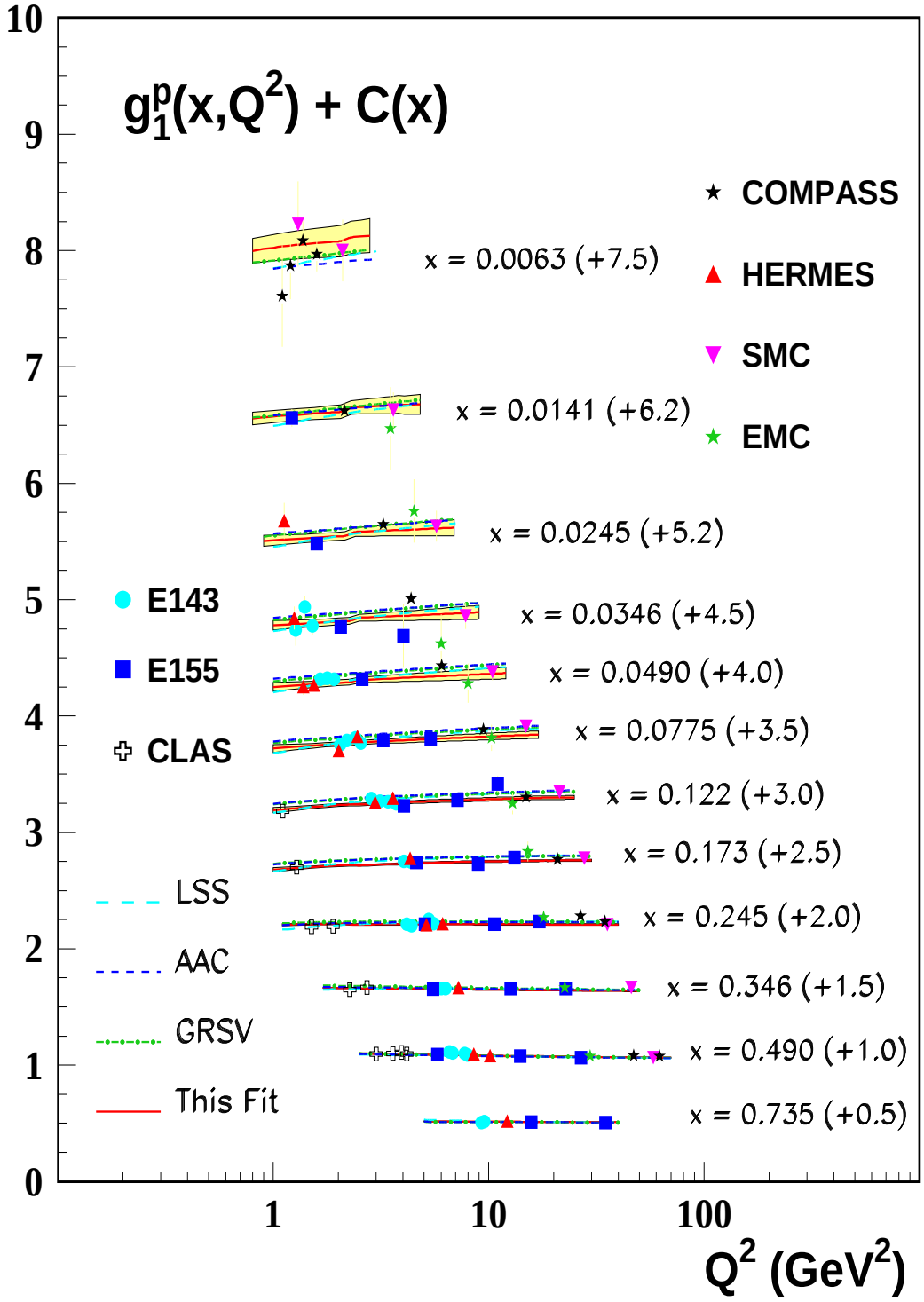

Figure 5: The spin–dependent structure function $xg_1^p(x,Q^2)$ as a function of x and Q^2. The experimental data are compared to the fit result (solid curve) with the statistical error bands (shaded areas). The curves obtained by GRSV (dashed-dotted) [19], AAC (short dashed) [18] and LSS (long dashed) [20] are shown for comparison.

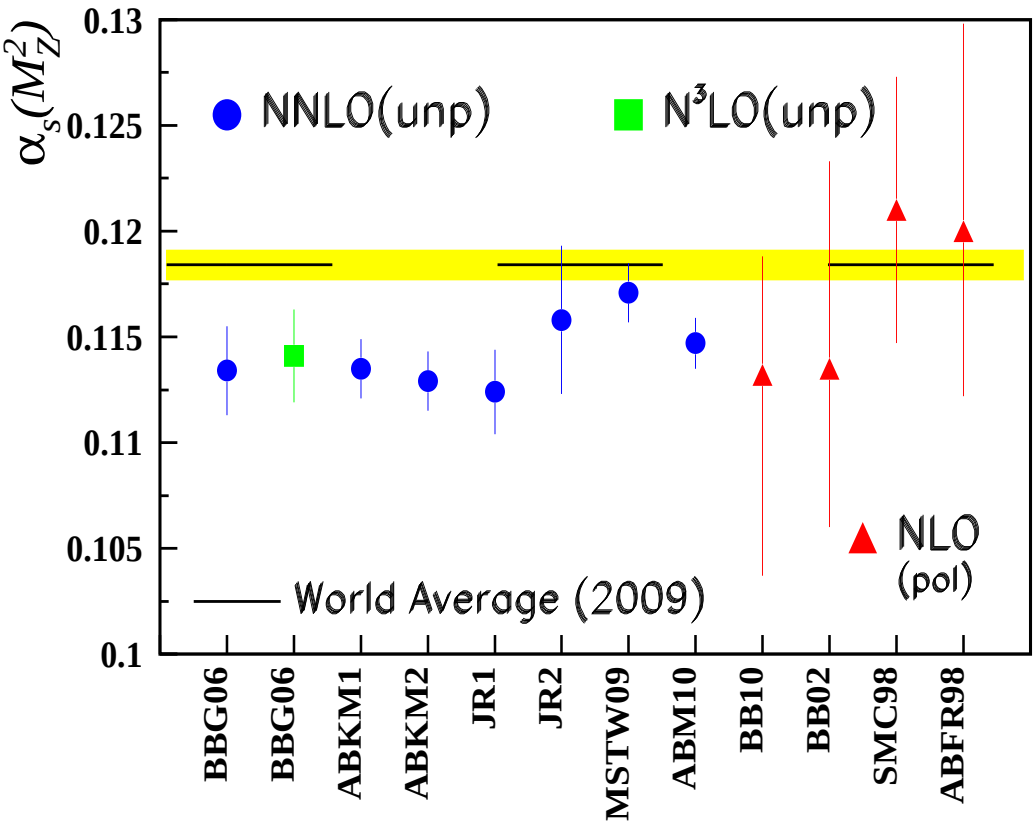

Figure 6: The strong coupling constant $\alpha_s(M_Z^2)$ from different DIS measurements, Eqs. (42–49,41) and Refs. [22,25,17]. The yellow band describes the weighted average of a wide range of $\alpha_s(M_Z)$ measurements [63].

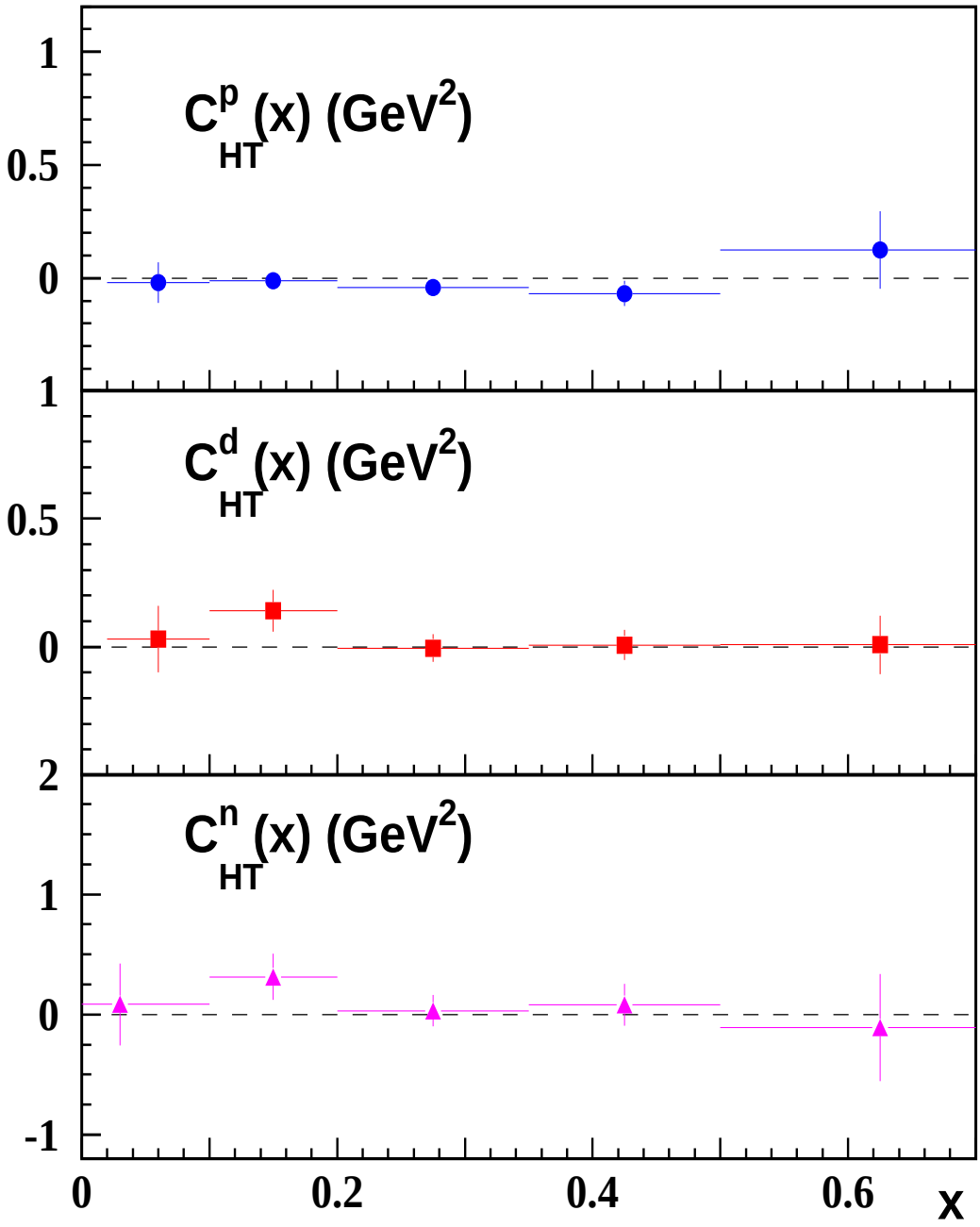

Figure 7: The higher twist coefficients $C_i^p(x)$, $C_i^d(x)$ and $C_i^n(x)$ as function of x.

References

[1] J. Ashman *et al.* [European Muon Collaboration], Phys. Lett. B **206** (1988) 364; Nucl. Phys. B **328** (1989) 1.

[2] P. L. Anthony *et al.* [E142 Collaboration], Phys. Rev. D **54** (1996) 6620 [arXiv:hep-ex/9610007].

[3] K. Ackerstaff *et al.* [HERMES Collaboration], Phys. Lett. B **404** (1997) 383 [arXiv:hep-ex/9703005].

[4] K. Abe *et al.* [E154 Collaboration], Phys. Rev. Lett. **79** (1997) 26 [arXiv:hep-ex/9705012].

[5] B. Adeva *et al.* [Spin Muon Collaboration], Phys. Rev. D **58** (1998) 112001.

[6] K. Abe *et al.* [E143 collaboration], Phys. Rev. D **58** (1998) 112003 [arXiv:hep-ph/9802357].

[7] A. Airapetian *et al.* [HERMES Collaboration], Phys. Rev. D **75** (2007) 012007 [arXiv:hep-ex/0609039].

[8] P. L. Anthony *et al.* [E155 Collaboration], Phys. Lett. B **463** (1999) 339 [arXiv:hep-ex/9904002].

[9] P. L. Anthony *et al.* [E155 Collaboration], Phys. Lett. B **493** (2000) 19 [arXiv:hep-ph/0007248].

[10] X. Zheng et al., The JLAB Hall A collaboration, Phys. Rev. **C70** (2004) 065207.

[11] V. Y. Alexakhin *et al.* [COMPASS Collaboration], Phys. Lett. B **647** (2007) 8 [arXiv:hep-ex/0609038].

[12] K. V. Dharmawardane *et al.* [CLAS Collaboration], Phys. Lett. B **641** (2006) 11 [arXiv:nucl-ex/0605028].

[13] The CLAS collaboration, private communication.

[14] M. G. Alekseev et al. [The COMPASS Collaboration], arXiv:1001.4654 [hep-ex].

[15] K. Abe *et al.* [E154 Collaboration], Phys. Lett. B **405** (1997) 180 [arXiv:hep-ph/9705344].

[16] J. Blümlein and A. Tkabladze, Nucl. Phys. B **553** (1999) 427 [arXiv:hep-ph/9812478].

[17] G. Altarelli, R. D. Ball, S. Forte and G. Ridolfi, Acta Phys. Polon. B **29** (1998) 1145 [arXiv:hep-ph/9803237];
S. Forte, M. L. Mangano and G. Ridolfi, Nucl. Phys. B **602** (2001) 585 [arXiv:hep-ph/0101192].

[18] Y. Goto *et al.* [Asymmetry Analysis collaboration], Phys. Rev. D **62** (2000) 034017 [arXiv:hep-ph/0001046];
M. Hirai, S. Kumano and N. Saito [Asymmetry Analysis Collaboration], Phys. Rev. D **69** (2004) 054021 [arXiv:hep-ph/0312112];
M. Hirai, S. Kumano and N. Saito, Phys. Rev. D **74** (2006) 014015 [arXiv:hep-ph/0603213];
M. Hirai and S. Kumano [Asymmetry Analysis Collaboration], Nucl. Phys. B **813** (2009) 106 [arXiv:0808.0413 [hep-ph]].

[19] M. Glück, E. Reya, M. Stratmann and W. Vogelsang, Phys. Rev. D **63** (2001) 094005 [arXiv:hep-ph/0011215].

[20] E. Leader, A. V. Sidorov and D. B. Stamenov, Eur. Phys. J. C **23** (2002) 479 [arXiv:hep-ph/0111267].

[21] E. Leader, A. V. Sidorov and D. B. Stamenov, Phys. Rev. D **80** (2009) 054026 [arXiv:0908.2390 [hep-ph]].

[22] J. Blümlein and H. Böttcher, Nucl. Phys. B **636** (2002) 225 [arXiv:hep-ph/0203155].

[23] S. Atashbar Tehrani and A. N. Khorramian, JHEP **0707** (2007) 048 [arXiv:0705.2647 [hep-ph]].

[24] D. de Florian, R. Sassot, M. Stratmann and W. Vogelsang, Phys. Rev. Lett. **101** (2008) 072001 [arXiv:0804.0422 [hep-ph]]; Phys. Rev. D **80** (2009) 034030 [arXiv:0904.3821 [hep-ph]].

[25] B. Adeva *et al.* [Spin Muon Collaboration], Phys. Rev. D **58** (1998) 112002.

[26] L. Del Debbio, A. Guffanti and A. Piccione, JHEP **0911** (2009) 060 [arXiv:0907.2506 [hep-ph]].

[27] J. Blümlein, H. Böttcher and A. Guffanti, Nucl. Phys. B **774** (2007) 182 [arXiv:hep-ph/0607200]; Nucl. Phys. Proc. Suppl. **135** (2004) 152 [arXiv:hep-ph/0407089].

[28] M. Glück, E. Reya and C. Schuck, Nucl. Phys. B **754** (2006) 178 [arXiv:hep-ph/0604116]; P. Jimenez-Delgado and E. Reya, Phys. Rev. D **79** (2009) 074023 [arXiv:0810.4274 [hep-ph]].

[29] A. D. Martin, W. J. Stirling, R. S. Thorne and G. Watt, Eur. Phys. J. C **64** (2009) 653 [arXiv:0905.3531 [hep-ph]].

[30] S. Alekhin, J. Blümlein, S. Klein and S. Moch, Phys. Rev. D **81** (2010) 014032 [arXiv:0908.2766 [hep-ph]].

[31] A. D. Watson, Z. Phys. **C12** (1982) 123;
W. Vogelsang, Z. Phys. **C50** (1991) 275.

[32] M. Buza, Y. Matiounine, J. Smith *et al.*, Nucl. Phys. **B485** (1997) 420; [hep-ph/9608342];
I. Bierenbaum, J. Blümlein, S. Klein, [arXiv:0706.2738 [hep-ph]] and in preparation.

[33] S. I. Alekhin, J. Blümlein, Phys. Lett. **B594** (2004) 299. [hep-ph/0404034].

[34] M. Lacombe, B. Loiseau, R. Vinh Mau, J. Cote, P. Pires and R. de Tourreil, Phys. Lett. B **101** (1981) 139;
W. W. Buck and F. Gross, Phys. Rev. D **20** (1979) 2361;
M. J. Zuilhof and J. A. Tjon, Phys. Rev. C **22** (1980) 2369;
R. Machleidt, K. Holinde and C. Elster, Phys. Rept. **149** (1987) 1;
A. Y. Umnikov, L. P. Kaptari, K. Y. Kazakov and F. C. Khanna, arXiv:hep-ph/9410241.

[35] R. Mertig and W. L. van Neerven, Z. Phys. C **70** (1996) 637 [arXiv:hep-ph/9506451];
W. Vogelsang, Phys. Rev. D **54** (1996) 2023 [arXiv:hep-ph/9512218].

[36] see e.g. : W. Furmanski and R. Petronzio, Z. Phys. C **11** (1982) 293 and references therein; G. T. Bodwin and J. W. Qiu, Phys. Rev. D **41** (1990) 2755.

[37] E. B. Zijlstra and W. L. van Neerven, Nucl. Phys. B **417** (1994) 61, [Erratum-ibid. B **426** (1994) 245; B **773** (2007) 105].

[38] J. Blümlein and S. Kurth, Phys. Rev. D **60** (1999) 014018 [arXiv:hep-ph/9810241]; J. A. M. Vermaseren, Int. J. Mod. Phys. A **14** (1999) 2037 [arXiv:hep-ph/9806280].

[39] J. Blümlein, Comput. Phys. Commun. **133** (2000) 76 [arXiv:hep-ph/0003100]; J. Blümlein and S. O. Moch, Phys. Lett. B **614** (2005) 53 [arXiv:hep-ph/0503188]; J. Blümlein, Comput. Phys. Commun. **180** (2009) 2218 [arXiv:0901.3106 [hep-ph]]; arXiv:0901.0837 [math-ph]; J. Ablinger, J. Blümlein, and C. Schneider, in preparation.

[40] M. Glück, E. Reya and A. Vogt, Z. Phys. C **48** (1990) 471.

[41] J. Blümlein and A. Vogt, Phys. Rev. D **58** (1998) 014020 [arXiv:hep-ph/9712546].

[42] J. Blümlein and A. Vogt, Phys. Lett. B **370** (1996) 149 [arXiv:hep-ph/9510410]; Phys. Lett. B **386** (1996) 350 [arXiv:hep-ph/9606254].

[43] J. Blümlein and A. Vogt, Acta Phys. Polon. B **27** (1996) 1309 [arXiv:hep-ph/9603450]; J. Bartels, B. I. Ermolaev and M. G. Ryskin, Z. Phys. C **72** (1996) 627 [arXiv:hep-ph/9603204]; Y. Kiyo, J. Kodaira and H. Tochimura, Z. Phys. C **74** (1997) 631 [arXiv:hep-ph/9701365]; J. Blümlein, arXiv:hep-ph/9909449; Lecture Notes in Physics **Vol. 546** (Springer, Berlin, 2000), pp. 42.

[44] M.J. Alguard et al., E80, Phys. Rev. Lett. **37** (1976) 1261; G. Baum et al., E130, Phys. Rev. Lett. **51** (1983) 1135.

[45] L.W. Withlow et al., Phys. Lett **B250** (1990) 193.

[46] M. Arneodo et al., NMC collaboration, Nucl. Phys. **B483** (1997) 3.

[47] K. Abe et al., E143, Phys. Lett. **B452** (1999) 194.

[48] M. Arneodo et al. (NMC), Phys. Lett. **B364** (1995) 107.

[49] D. Adams et al., SMC collaboration, Phys. Lett. **B336** (1994) 125.

[50] K. Abe et al. (E154)), Phys. Lett. **B404** (1997) 377.

[51] K. Abe et al. (E155x)), Phys. Lett. **B553** (2003) 18.

[52] S. Wandzura, F. Wilczek, Phys. Lett. **B72** (1977) 195.

[53] A. Piccione, G. Ridolfi, Nucl. Phys. **B513** (1998) 301, [hep-ph/9707478].

[54] R. G. Roberts, G. G. Ross, Phys. Lett. **B373** (1996) 235, [hep-ph/9601235]; J. Blümlein, N. Kochelev, Nucl. Phys. **B498** (1997) 285, [hep-ph/9612318]; Phys. Lett. **B381** (1996) 296, [hep-ph/9603397].

[55] J. Blümlein and D. Robaschik, Nucl. Phys. B **581** (2000) 449 [arXiv:hep-ph/0002071].

[56] J. Blümlein and D. Robaschik, Phys. Rev. **D65** (2002) 096002. [hep-ph/0202077].

[57] J. Blümlein, V. Ravindran and W. L. van Neerven, Phys. Rev. D **68** (2003) 114004 [arXiv:hep-ph/0304292].

[58] F. James, CERN Program Library, Long Writeup D506.

[59] J. Pumplin, D. R. Stump, J. Huston *et al.*, JHEP **0207** (2002) 012, [hep-ph/0201195].

[60] C. Amsler et al. (Particle Data Group), Phys. Lett. B **667** (2008) 1.

[61] A. Airapetian *et al.* [HERMES Collaboration], Phys. Rev. **D71** (2005) 012003, [hep-ex/0407032].

[62] M. Glück, E. Reya, A. Vogt, Eur. Phys. J. **C5** (1998) 461, [hep-ph/9806404].

[63] S. Bethke, Eur. Phys. J. C **64** (2009) 689 [arXiv:0908.1135 [hep-ph]].

[64] F. D. Aaron *et al.* [H1 Collaboration and ZEUS Collaboration], JHEP **1001** (2010) 109 [arXiv:0911.0884 [hep-ex]].

[65] S.I. Alekhin, J. Blümlein, and S.-O. Moch, DESY 10–065, in preparation.

[66] H1 and ZEUS collab. (V. Radescu et al.), Combined H1 and ZEUS Fits Using Low Energy Data, talk, DIS 2010, Florence, April 2010.

[67] R. Abbate, M. Fickinger, A. Hoang, V. Mateu and I. W. Stewart, arXiv:1004.4894 [hep-ph]; MPP-2010-7, MIT-CTP 4101 to appear.

[68] T. Gehrmann, M. Jaquier and G. Luisoni, Eur. Phys. J. C **67** (2010) 57 [arXiv:0911.2422 [hep-ph]].

[69] D. B. Renner, arXiv:1002.0925 [hep-lat].

[70] H. W. Lin, T. Blum, S. Ohta, S. Sasaki and T. Yamazaki, Phys. Rev. D **78** (2008) 014505 [arXiv:0802.0863 [hep-lat]].

[71] Y. Aoki *et al.*, Phys. Rev. D **72** (2005) 114505 [arXiv:hep-lat/0411006];
J. Zanotti, private communication for QCDSF;
T. Yamazaki *et al.*, Phys. Rev. D **79** (2009) 114505 [arXiv:0904.2039 [hep-lat]];
C. Gattringer, C. Hagen, C. B. Lang, M. Limmer, D. Mohler and A. Schäfer, Phys. Rev. D **79** (2009) 054501 [arXiv:0812.1681 [hep-lat]];
D. Mohler, private communication for BGR;
J. Negele, private communication for LHPC;
T. Korzec, private communication for ETMC.

[72] Ph. Hägler *et al.* [LHPC Collaborations], Phys. Rev. D **77** (2008) 094502 [arXiv:0705.4295 [hep-lat]];
J. D. Bratt *et al.* [LHPC Collaboration], arXiv:1001.3620 [hep-lat].

[73] G. Schierholz, private communication.

[74] M. Göckeler et al., QCDSF collaboration, Phys. Rev. **D53** (1996) 2317; Phys. Lett. **B414** (1997) 340; `hep-ph/9711245`; Phys. Rev. **D63** (2001) 074506;
S. Capitani et al., Nucl. Phys. (Proc. Suppl.) **B79** (1999) 548;
S. Güsken et al., SESAM collaboration, `hep-lat/9901009`;
D. Dolgov *et al.* [LHPC collaboration and TXL Collaboration], Phys. Rev. D **66** (2002) 034506 [arXiv:hep-lat/0201021].

[75] M. Virchaux and A. Milsztajn, Phys. Lett. B **274** (1992) 221.

[76] S.I. Alekhin, Phys. Rev. D **68** (2003) 014002 [arXiv:hep-ph/0211096].

[77] J. Blümlein and H. Böttcher, Phys. Lett. B **662** (2008) 336 [arXiv:0802.0408 [hep-ph]].

[78] S.I. Alekhin, S. Kulagin and R. Petti, The low-Q deep-inelastic scattering data in the global fit of PDFs, Proc. 15th International Workshop on Deep-Inelastic Scattering and Related Subjects (DIS2007), Munich, Germany, 2007, Vol. 1, pp. 313.